CENTER FOR INFRASTRUCTURE ENGINEERING STUDIES

Assessment of Bridge Technologies Through Field Testing: In-Situ Load Testing of Bridges B-20-148 and B-20-149, Fond du Lac, WI

By

Eli Hernandez
Nestore Galati
Antonio Nanni

UTC R133B

University Transportation Center Program at

The University of Missouri-Rolla

Disclaimer

The contents of this report reflect the views of the author(s), who are responsible for the facts and the accuracy of information presented herein. This document is disseminated under the sponsorship of the Department of Transportation, University Transportation Centers Program and the Center for Infrastructure Engineering Studies UTC program at the University of Missouri - Rolla, in the interest of information exchange. The U.S. Government and Center for Infrastructure Engineering Studies assumes no liability for the contents or use thereof.

Technical Report Documentation Page

1. Report No.	2. Government Accession No.	3. Recipient's Catalog No.
UTC R133B		

4. Title and Subtitle	5. Report Date
Assessment of Bridge Technologies through Field Testing: In-situ load testing of Bridges B-20-148 and B-20-149, Fond du Lac, WI	December 2005
	6. Performing Organization Code

7. Author/s	8. Performing Organization Report No.
Eli Hernandez, Nestore Galati, and Antonio Nanni	00001342

9. Performing Organization Name and Address	10. Work Unit No. (TRAIS)
Center for Infrastructure Engineering Studies/UTC program University of Missouri - Rolla 223 Engineering Research Lab Rolla, MO 65409	11. Contract or Grant No. DTRS98-G-0021

12. Sponsoring Organization Name and Address	13. Type of Report and Period Covered
U.S. Department of Transportation Research and Special Programs Administration 400 7th Street, SW Washington, DC 20590-0001	Final
	14. Sponsoring Agency Code

15. Supplementary Notes

16. Abstract

The scope of this project is the evaluation of two twin bridges having numbers B-20-148 and B-20-149, respectively, located on US Highway 151, in Fond du Lac County, Wisconsin. Bridge B-20-148 was constructed utilizing a cast in place Fiber Reinforced Polymer (FRP) Reinforced Concrete (RC) Deck while Bridge B-20-149 was built using a conventional cast in place RC deck.
To better evaluate the load-carrying capacity of the bridges, a nondestructive field test was conducted. The bridges were tested statically using six dump trucks. The bridges deflections were measured using a Robotic Tacheometry System (RTS), while the strains at critical locations were measured by means of electrical resistive strain gages. The RTS is a noncontact deflection measurement technique that offers the capability to measure the spatial coordinates of discrete points on a structure in three dimensions without having to touch the object.
A Finite Element Method (FEM) Model was developed to represent the behavior of the bridge and was used to determine the actual load rating of the structure and its safety over time. The comparison between analytical results obtained according to AASTHO standard specifications, FEM modeling and experimental allowed establishing a good understanding of the bridges performance.

17. Key Words	18. Distribution Statement
assessment, bridge monitoring, concrete deck, high performance steel, in-situ load test, static load test, structural evaluation, thermal effect, total station.	No restrictions. This document is available to the public through the National Technical Information Service, Springfield, Virginia 22161.

19. Security Classification (of this report)	20. Security Classification (of this page)	21. No. Of Pages	22. Price
unclassified	unclassified		

Form DOT F 1700.7 (8-72)

ACKNOWLEDGMENTS

The project was made possible with the financial support received from the University of Wisconsin Madison and UMR - University Transportation Center on Advanced Materials and Center for Infrastructure Engineering Studies at the University of Missouri-Rolla. The authors would like to acknowledge Dr. Larry Bank and Dr. Michael Oliva at University of Wisconsin – Madison for their assistance in the different parts of the project.

TABLE OF CONTENTS

TABLE OF CONTENTS vi
LIST OF FIGURES vii
LIST OF TABLES viii
NOTATIONS I
1 INTRODUCTION 2
1.1 Background 2
1.1.1 Pultruded Grid and Stay-in-Place (SIP) Form Panels for the Rapid Construction of Bridge Decks 2
1.1.2 Diagnostic Load Testing 2
1.1.3 Robotic Tacheometry Systems in Diagnostic Load Tests 3
1.2 Bridges Description 4
1.2.1 Bridge B-20-148 4
1.2.2 Bridge B-20-149 4
1.3 Objectives 8
1.4 Equipment Description 8
1.4.1 Total station 8
1.4.2 Data Acquisition System: (DAS) 8
2 FIELD EVALUATION 10
2.1 Bridge Instrumentation 10
2.1.1 Bridge B-20-148 10
2.1.2 Bridge B-20-149 12
2.2 Load Testing Methodology 13
2.2.1 Bridge B-20-148 13
2.2.2 Bridge B-20-149 17
2.3 Test Results 19
2.3.1 Bridge B-20-148 19
2.3.2 Bridge B-20-149 21
2.4 Discussion of Results 23
2.4.1 Bridge B-20-148 23
2.4.2 Bridge B-20-149 26
2.5 Finite Element Method Simulations 29
2.5.1 Bridge B-20-148 31
2.5.2 Bridge B-20-149 35
3 SUMMARY AND CONCLUSIONS 37
4 REFERENCES 38

LIST OF FIGURES

Figure 1 Bridge B-20-148 Details (all dimensions in mm) 5
Figure 2 Bridge B-20-149 details (all dimensions in mm) 6
Figure 3 Side View of Bridges B-20-148 (Front) and B-20-149 (Back) 6
Figure 4 Framing Plan (all dimensions in mm) 7
Figure 5 Total Station 8
Figure 6 Data Acquisition System ("Orange Box") 9
Figure 7 Target Positions: Plan View of Bridge B-20-148 (Drawing not to scale) 10
Figure 8 Targets Mounted on Bridge Girders 10
Figure 9 Cut Away View of Strain Gage Location on FRP Reinforcement (Conachen, 2005) ... 11
Figure 10 Cross Section at Mid-span Showing Strain Gage Profile Through Depth of Slab (Conachen, 2005) 11
Figure 11 H-20 Dump Trucks 12
Figure 12 Target Positions of Bridge B-20-149: Plan View (Drawing not in scale) 12
Figure 13 Transversal Position of the Trucks 14
Figure 14 Truck Configurations During Load Testing of Bridge B-20-148 (Drawing not to scale) 15
Figure 15 Trucks Aligned During Test 1 16
Figure 16 Transversal Position of the Trucks 17
Figure 17 Truck Configurations During Load Testing of Bridge B-20-149 (Drawing not to scale) 18
Figure 18 Trucks Aligned on Test 1 19
Figure 19 Longitudinal Deflections of Girder 2 Tests 1 to 4 19
Figure 20 Vertical Deflections at L/2 from West Abutment Tests 1 to 4 20
Figure 21 Longitudinal Deflections of Girder 6 Tests 1 to 4 20
Figure 22 Longitudinal Deflections of Girder 8 Tests 1 to 3 21
Figure 23 Vertical Deflections at L/2 from west abutment Stops 1 to 3 21
Figure 24 Longitudinal Deflections of Girder 4 Tests 1 to 3 22
Figure 25 Comparison Between AASTHO Provisions and Experimental Results 24
Figure 26 Comparison Between AASHTO and Experimental GDF at Mid-span (Two Lanes Loaded, Tests 1 and 2) 25
Figure 27 Comparison Between AASHTO and Experimental GDF at Mid-span (One Lane Loaded, Tests 3 and 4) 25

Figure 28 Comparison Between AASTHO Provisions and Experimental Results 27

Figure 29 Comparison Between AASHTO and Experimental GDF at Mid-span (Two Lanes Loaded, Test 2) 28

Figure 30 Comparison Between AASHTO and Experimental GDF at Mid-span (One Lane Loaded, Test 1 and 3)..... 28

Figure 31 Finite Element Model of Bridge B-20-148 29

Figure 32 Finite Element Model of Bridge B-20-149 30

Figure 33 Comparison between FEM Model and Experimental Results (Test 1 to 4)..... 31

Figure 34 Comparison between FEM Model and Experimental Results (Vertical Deflections at Mid-span, Tests 1 to 4) 32

Figure 35 Comparison Between Strain Gage Readings and FEM and Results 33

Figure 36 Plot Contour of Strain ε_{22} (Direction of the Deck FRP Reinforcement)..... 34

Figure 37 Comparison between FEM Model and Experimental Results (Stops 1 to 3)..... 35

Figure 38 Comparison between FEM Model and Experimental Results (Vertical Deflections at Mid-span, Tests 1 to 3) 36

LIST OF TABLES

Table 1 Weight of Trucks Used for Test of Bridge B-20-148..... 12

Table 2 Trucks Used for Test of Bridge B-20-149..... 13

Table 3 GDFs as per AASHTO LRFD Bridge Design Specifications (1998) 23

Table 4 Input Data for Calculations of GDFs (AASHTO, 1998)..... 23

Table 5 GDFs as per AASHTO LRFD Bridge Design Specifications (1998) 26

Table 6 Input Data for Calculations of GDFs (AASHTO, 1998)..... 26

Table 7 Comparison between Stress Results of FRP Components and Allowable Stress..... 34

NOTATIONS

A	:	Cross sectional area of girder, mm^2
A_b	:	Cross sectional area of concrete barrier, mm^2
E_c	:	Modulus of elasticity of concrete girder, MPa
E_{cs}	:	Modulus of elasticity of girder, MPa
I	:	Moment of inertia of the concrete girder section, mm^4
K_g	:	Longitudinal stiffness parameter, mm^4
L	:	Span length, mm
P_1	:	Dump truck front axle load, kN
P_2	:	Dump truck rear axle load, kN
S	:	Girder spacing, mm
e_g	:	Distance between center of gravity of girder section and concrete deck, mm
f_y	:	Steel yield strength, MPa
m	:	Multiple presence factor
t_s	:	Thickness of concrete deck, mm
$w_{overhang}$	:	Overhang width from exterior girder center line, mm
δ_i	:	Deflection of ith girder, mm
GDF	:	Girder distribution factor
θ	:	Skew angle
d_e	:	Distance between center of exterior girder and interior edge of barrier
n	:	Modular ratio between beam and slab, $n = \frac{E_s}{E_{cs}}$

1 INTRODUCTION

1.1 Background

1.1.1 Pultruded Grid and Stay-in-Place (SIP) Form Panels for the Rapid Construction of Bridge Decks

The Federal Highway Administration (FHWA) has reported that in the United States there are over half a million of bridges in service and that more than twenty five percent of these bridges are considered deficient. Among the principal reasons ascribed to the structural deterioration of these existing bridges are corrosion of reinforcing steel due to chloride ion penetration, aging of materials and inadequate maintenance of the infrastructure. Deficient bridges are usually posted, repaired or replaced causing elevated costs to the nation. The impact of the economic and social costs associated with bridge deck rehabilitation and replacement presents a necessity to develop durable structural systems that can be rapidly installed. Fiber Reinforced Polymer (FRP) materials are very attractive to engineers because of their high resistance to electromechanical corrosion. This feature makes the material particularly advantageous in high-alkali environments such as concrete exposed to saline seawater or deicing salts (Conachen 2005). Although the glass fibers by themselves are susceptible to alkaline degradation, their polymer-resin encasement makes the material essentially inert.

To date, extensive research has demonstrated the effectiveness of using pultruded FRP gratings as internal reinforcement of bridge decks (Bank et al. 1992, Bank and Xi 1993, 1995). Together with durability, the key feature of the proposed solutions is the quickness of installation. Similarly, the use of pultruded Glass FRP (GFRP) bars as internal reinforcement of concrete decks and railings ideally eliminates the problem of corrosion and also simplifies the installation process (Bradberry 2001, Buth et al. 2003, El-Salakawi et al. 2003).

Extensive research and development work funded through the FHWA Innovative Bridge Research and Construction (IBRC) project demonstrated the feasibility of using prefabricated bi-directional FRP grids in the rapid construction of steel-free bridge decks. This technology was recently implemented in pilot field applications in Wisconsin, U.S.A. (Conachen, 2005). The concept of the proposed system consists on using double layer FRP grids in large modular sections that can be easily lifted into place with a crane.

The modular 3-D FRP grids, or FRP cages are fabricated by pultruding the components and cutting them to proper lengths (Bank et al., 2004). There are four types of pultruded sections, one for the main bars, one for the shear connectors and two for the cross-rods(Conachen, 2005).

1.1.2 Diagnostic Load Testing

Field-testing is an important topic in the validation of innovative infrastructure as well as in the assessment of deficient structures. There is a need for accurate and inexpensive diagnostics methods that allow the determination of the actual load carrying capacity of the structures. In order to predict the response of a bridge, its evaluation must accurately expose its present load carrying capacity and should predict loads and any further changes of its capacity (deterioration) during the applicable time life span.

Experimental load testing on a bridge can be categorized as either diagnostic or proof test. In a diagnostic test, a predetermined load, typically near the bridge's rated capacity, is placed at

several different locations along the bridge and its behavior is obtained. The measured response is used to develop numerical models of the bridge to estimate its maximum allowable load. In a proof test, incremental loads are applied to the bridge until either a target load is reached or a predetermined limit state is exceeded. Using the maximum load reached, the capacity of the bridge can be determined. While diagnostic tests provide only an estimate of a bridge's capacity, they have several practical advantages including a lower cost, a shorter testing time, and less disruption to traffic. Because of these advantages, diagnostic testing was used in this evaluation. Frequently, diagnostic load tests reveal strength and serviceability characteristics that exceed predicted parameters. Usually, these parameters are very conservative in predicting lateral load distribution factors and the influence of other structural attributes. As a result, the predicted rating factors are typically conservative (Chajes et al. 1997). This difference can be attributed to the existence of "beneficial factors", such as parapet stiffening, contribution of secondary members, diaphragm action, concrete hardening, unintended composite action and unintended bearing restraints that are usually neglected in a new bridge design and analytical capacity rating (Cai et al. 2003).

A difficulty of testing and evaluating bridges in the field is the measurement of vertical deflection. The use of instruments such as mechanical dial gages, linear potentiometers, linear variable differential transducers (LVDTs), and other similar types of deflection transducers is usually not feasible. Access under a bridge structure sometimes is limited due to several conditions; for instance, the necessity to erect temporary supports to mount and setup the measurement instruments to the ground or the presence of a natural creek under the bridge. These difficulties can be eliminated by using a Robotic Tacheometry System (RTS), which is a noncontact deflection measurement technique. RTS offers the capability to measure the spatial coordinates of discrete points on a bridge in three dimensions without having to touch the structure. In this research, the RTS was used to monitor the deflection of points located along the bridge girder.

1.1.3 Robotic Tacheometry Systems in Diagnostic Load Tests

RTS also called Total stations have been used to measure the movement of structures and natural processes with good results (Hill and Sippel 2002; Kuhlmann and Glaser 2002). Leica Geosystems quotes accuracies of better than 1mm for their bridge and tunnel surveys where a remote system is used to log measurements six times daily via a modem, with measurements still possible at peak times. Kuhlmann and Glaser (2002) used a reflectorless total station to monitor the long-term deformation of bridges. Measurements were taken of the whole bridge every six years and statistical tests were used to confirm if the points had moved. Hill and Sippel (2002) used a total station and other sensors to measure the deformation of the land in a landslide region. Merkle (2004) used the total station as part of a 5-year monitoring program for the in-situ load testing prior to and after the strengthening of five existing concrete bridges, geographically spread over three Missouri Department of Transportation (MODOT) districts. There are advantages and disadvantages of using a total station for dynamic deformation monitoring. The advantages include the high accuracy as quoted above, the automatic target recognition which provides precise target pointing (Hill and Sippel 2002) and the possibility of measuring indoors and in urban canyons (Radovanovic and Teskey 2001). The disadvantages include the low sampling rate (Meng 2002), problems with measurement in adverse weather conditions (Hill and

Sippel 2002) and the fact that a clear line of sight is needed between the total station and the prism.
Radovanovic and Teskey (2001) conducted experiments to compare the performance of a robotic total station with GPS. This experiment was conducted because GPS is not an option in many application areas such as indoors. Total stations are now capable of automatic target recognition and they can track a prism taking automatic measurements of angles and distances once lock has been established manually. It was found that the total station performed better than GPS in a stop and go situation, where measurements were taken of a moving object only when it was stationary. In a completely kinematic situation, GPS performed the best. It was found that there were two main problems with the total station in kinematic mode. These problems were basically a low EDM accuracy caused by a ranging error that was linearly dependent upon the line of sight velocity, and an uneven sampling rate over time worsened by no time tagging.

1.2 Bridges Description

The bridges under investigation are over the De Neuve Creek on U.S. Highway 151 in Fond du Lac, Wisconsin. Both bridges were completed during April 2004 and were designed for the controlling truck load known as MS18 with military 106 KN tandem axles.

1.2.1 Bridge B-20-148

Bridge B-20-148 carries two lanes of traffic and consists of a single span having a length of 39.62 m and width of 13.71 m. A skew angle of 25° was required to accommodate the angle of intersection between the highway and the creek. The cross section consists of seven 16459-mm (54-inch) deep by 14630-mm (48-inch) wide flange bulb tee Prestressed Concrete (PC) girders equally spaced, supporting an 8-inch thick FRP reinforced cast in place concrete deck. Cross section details of the PC girders of the bridge B-20-148 are presented in Figure 1 (Jacobson 2004 and Conachen 2005 give additional details about the design and construction of this bridge).

1.2.2 Bridge B-20-149

Bridge B-20-149 also carries two lanes of traffic and consists of a single span with the same length of bridge B-20-148, a width of 16.95m., and a skew angle of 27°45’. The cross section of this bridge consists of nine 16459-mm (54-inch) deep by 14630-mm (48-inch) wide flange bulb tee PC girders equally spaced, supporting an 8-inch thick cast in place conventional RC deck. Cross section details of the PC girders of bridge B-20-149 are presented in Figure 1. Figure 2 displays the cross section and details of this bridge.

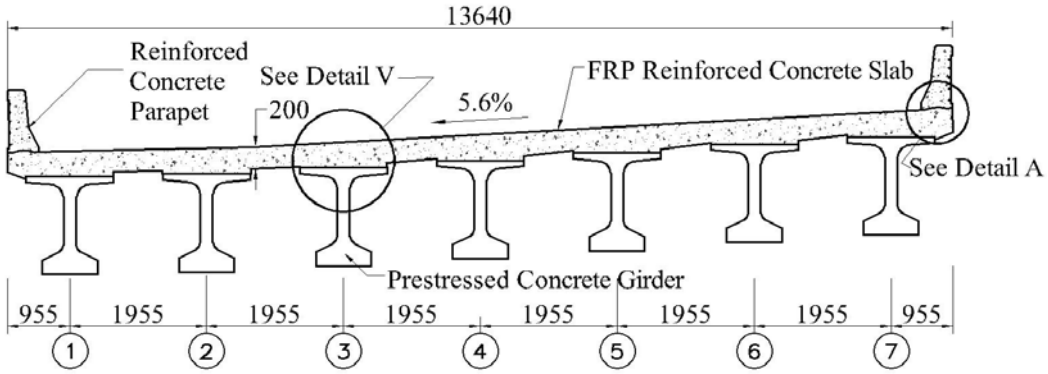

a) Cross Section of Bridge (drawing not in scale)

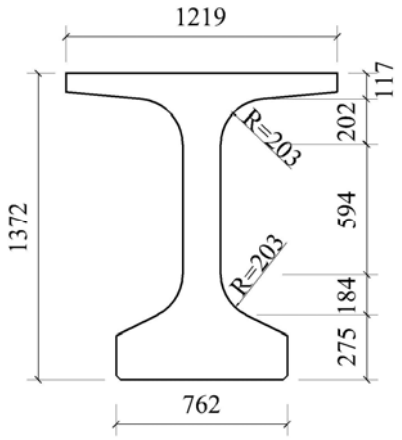

b) Cross Section of the Girders

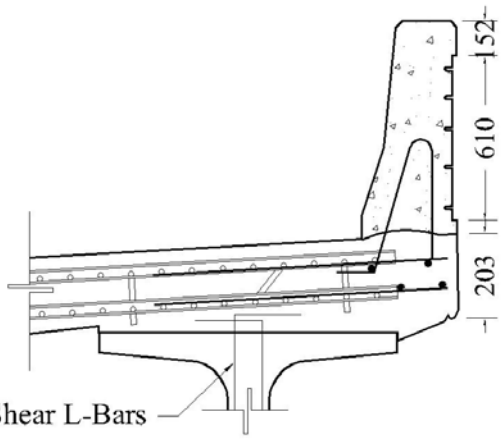

c) Detail A

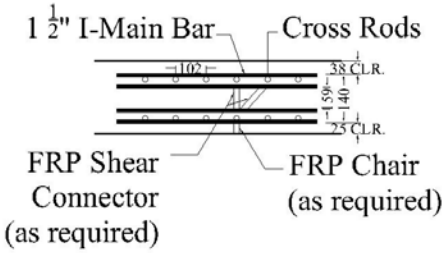

d) Detail V (drawing not in scale)

Figure 1 Bridge B-20-148 Details (all dimensions in mm)

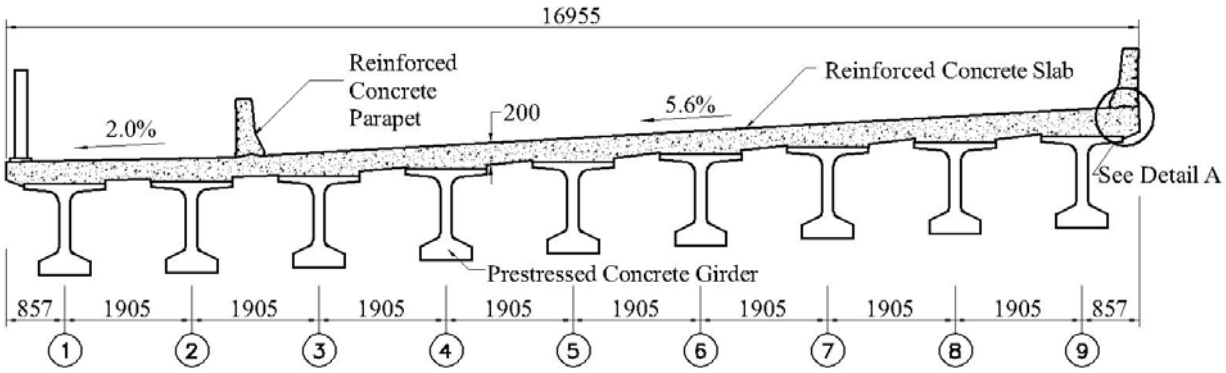

a) Cross Section of Bridge B-20-149 (drawing not in scale)

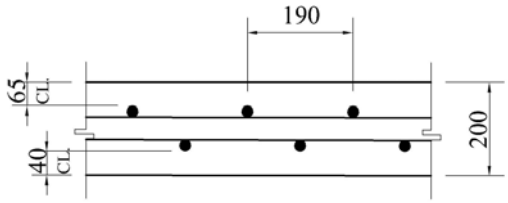

c) Detail B (drawing not in scale)

Figure 2 Bridge B-20-149 details (all dimensions in mm)

A photograph of the structure of both bridges is exhibited in Figure 3.

a) Bridge B-20-148

b) Bridge B-20-149

Figure 3 Side View of Bridges B-20-148 (Front) and B-20-149 (Back)

The plan view and typical diaphragm of both bridges are detailed in Figure 4.

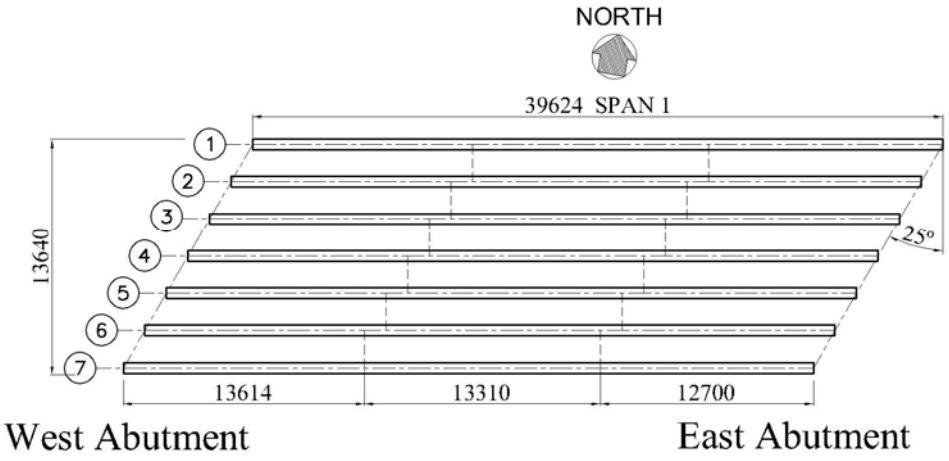

a) Plan View of Bridge B-20-148

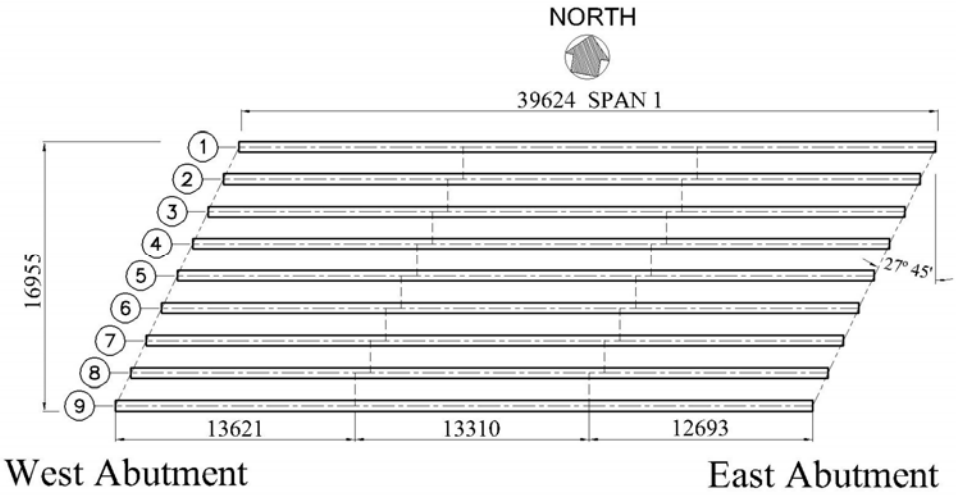

a) Plan View of Bridge B-20-149 (Drawing not in scale)

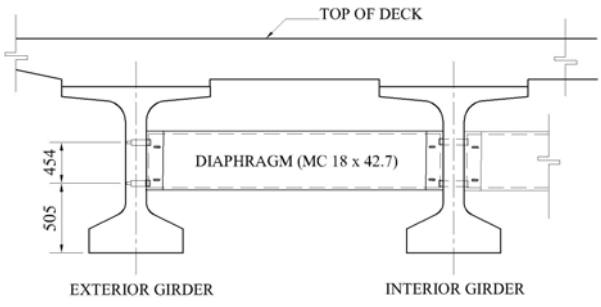

b) Typical Diaphragm (During Construction Phase of Bridges)

Figure 4 Framing Plan (all dimensions in mm)

1.3 Objectives

The scope of this project is the evaluation of two bridges built in Fond du Lac, Wisconsin, having number B-20-148 and B-20-149. To better evaluate the load-carrying capacity of the bridges, a nondestructive field test was conducted. A comparison between analytical results obtained according to AASTHO standard specifications, FEM modeling and experimental results was carried out in order to establish a good understanding of the bridges performance.

1.4 Equipment Description

1.4.1 Total station

The RTS used in this project is a Leica TCA2003 (www.leica-geosystems.com) as shown in Figure 5. The instrument sends a laser ray to reflecting prisms (see Figure 8) mounted on the structure to be monitored. By means of a triangulation with fixed reference points placed outside the structure. The RTS can determine how much the structure has moved in a three-dimensional array with an accuracy of 0.5 sec on angular measurements and 1mm+1ppm on distance measurements, in average atmospheric conditions.

Figure 5 Total Station

For this experimental program, strain gages were also used to characterize the bridges' response. In order to read the data from the strain gages, a custom-made data acquisition system was used. The system is able to read data up to 100 Hz.

1.4.2 Data Acquisition System: (DAS)

The DAS is a portable unit, suitable for use in field testing of structures. It is capable of recording 32 high-level channels of data, 16 strain channels, and 32 thermocouple channels, as well as interfacing a Leica Total Station surveying instrument (See Figure 6).

Figure 6 Data Acquisition System (“Orange Box”)

The high-level channels may consist of DC LVDT's, string transducers, linear potentiometers, or any other +/- 10 Volt DC signal. The strain channels can be used to monitor and record strain gage signals, load cells, strain-based displacement transducers, or any strain based signal. The 32 thermocouple channels are configured for type T thermocouples.
The unit consists of a shock-mounted transport box, with removable front and rear covers. Removal of the front cover exposes the computer keyboard and LED display, as well as the front panel of the data acquisition equipment. Removal of the back panel exposes the connector bay, where cables from all the transducers terminate.
The data acquisition system is comprised of National Instruments equipment, listed below:

1. A PXI-1010 SCXI combination unit, which houses the industrial-grade 2.2 GHz Pentium 4 computer, floppy drive, and CDR/W module;
2. A PXI-6030E Analog to Digital converter module for doing the A/D conversion in the system;
3. A pair of SCXI-1520 modules to interface strain based sensors;
4. A SCXI-1102B module for multiplexing high-level sensors;
5. A SCXI-1102B module for multiplexing thermocouple sensors;
6. I/O devices in order to connect additional peripherals and other data acquisition systems such as a Leica Total Station surveying instrument.

The entire DAS is controlled by LabVIEW software, which allows control of data rate, sensor selection and calibration, and display of the data.

2 FIELD EVALUATION

2.1 Bridge Instrumentation

2.1.1 Bridge B-20-148

Fourteen prisms (also called targets) were mounted along the girders in Bridge B-20-148 as shown in Figure 7. While target 6 and targets 12 to 14 provided the longitudinal deformed shape along internal Girder 2, target 2 and targets 8 to 10 provided the longitudinal deformed shape along internal Girder 6. The remaining targets were distributed transversally in order to determine the distribution of loads among the girders at mid-span. Additionally, three targets were mounted on tripods as reference points for triangulation.

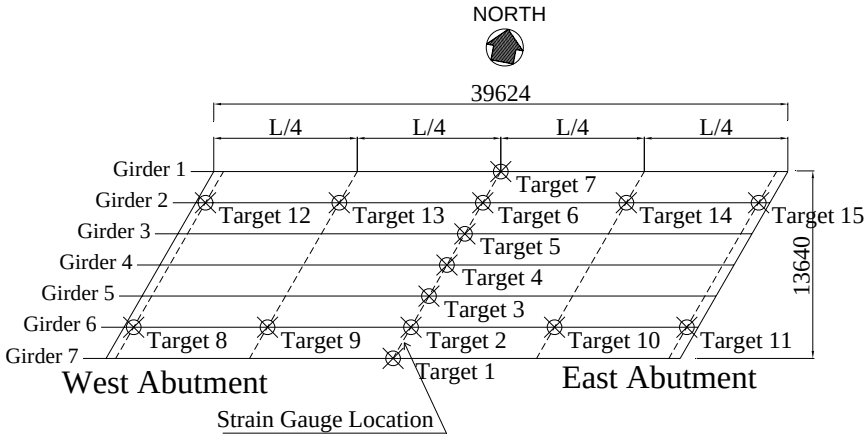

Figure 7 Target Positions: Plan View of Bridge B-20-148 (Drawing not to scale)

The targets were magnetically mounted on the structure prior to testing and this required the installation of steel plates on the structure at the corresponding positions. The steel plates were glued to the girders using an epoxy resin and, as an additional safety measure; they were mechanically fastened by using two bolts.

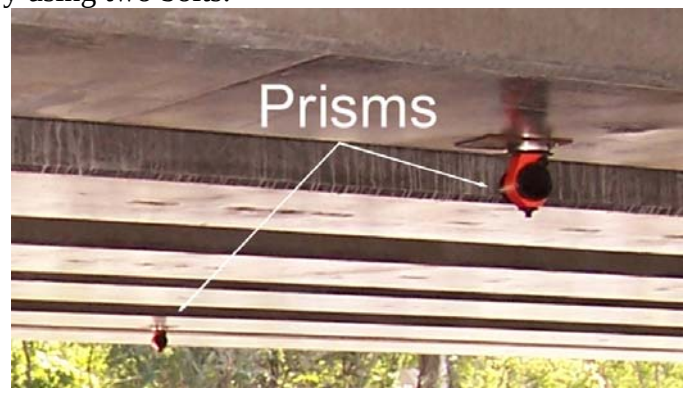

Figure 8 Targets Mounted on Bridge Girders

The connections of steel plates and pipes to the superstructure were designed to carry their own weight plus the weight of the targets with a safety factor equal to four.
The research team of the UW installed strain gages during the construction phase of the bridge, and their locations are presented in Figure 9 and Figure 10 (Conachen, 2005).

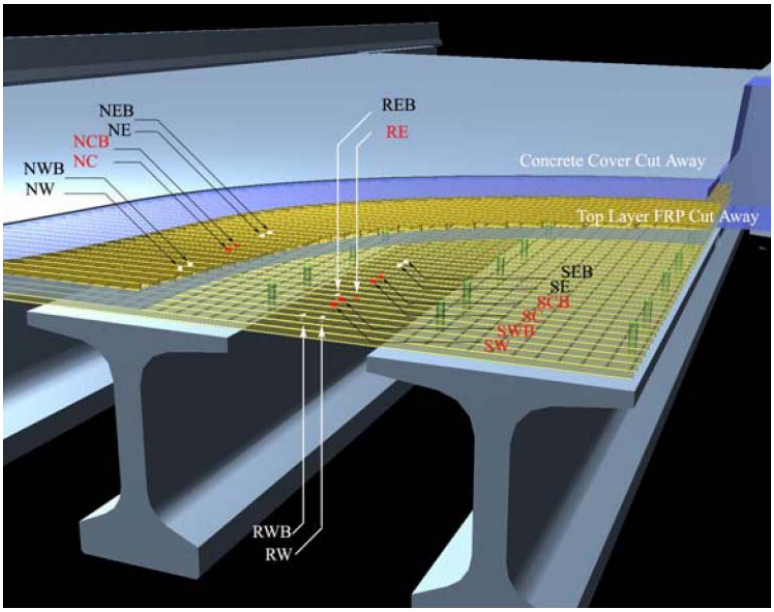

Figure 9 Cut Away View of Strain Gage Location on FRP Reinforcement (Conachen, 2005)

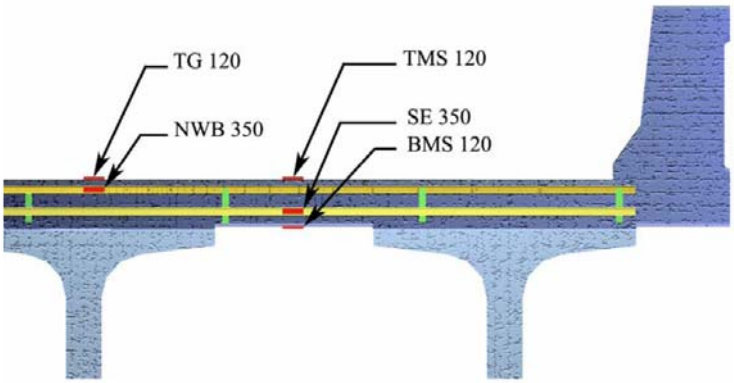

Figure 10 Cross Section at Mid-span Showing Strain Gage Profile Through Depth of Slab (Conachen, 2005)

The load test was carried out by using six fully loaded H-20 dump trucks that were weighted before test. The sketch in Figure 11b shows the average dimensions of the trucks used for the load test. All trucks were weighted before testing and coded with a number. Table 1 summarizes the weights and load distribution between front and rear axles of the trucks used for the test. The value P_2 in Table 1 corresponds to the weight of each of the rear axles, which means that the total rear weight of the truck will be twice P_2. The bridge was loaded using a train of trucks and the average distance between the front axle of a truck and the rear axle of the truck in front of it was 2.5 m.

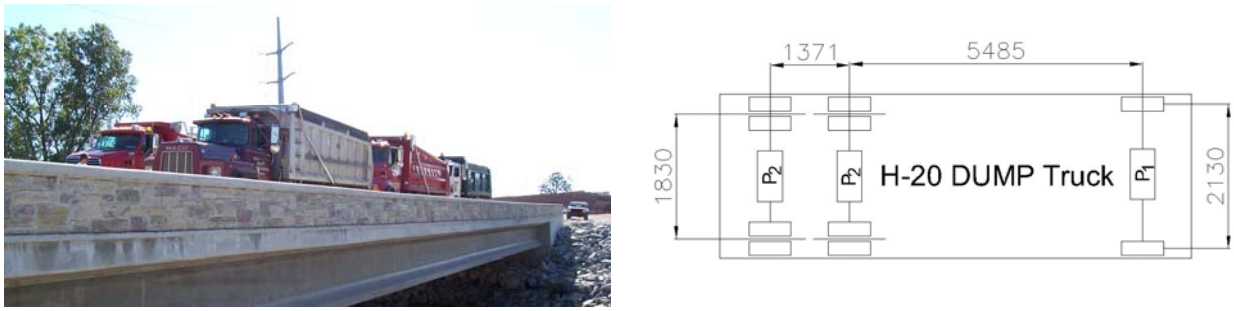

a) Trucks on Site b) Trucks Geometry (all dimensions in mm)

Figure 11 H-20 Dump Trucks

Table 1 Weight of Trucks Used for Test of Bridge B-20-148

Truck Code	Total Weight (kN)	Front Axle (P_1) (kN)	Each Rear Axle (P_2) (kN)
1	325.4	108.9	108.25
2	330.6	118.6	106.0
3	331.2	109.9	110.65
4	329.5	109.7	109.9
5	342.6	145.9	98.35
6	338.8	99.7	119.55

2.1.2 Bridge B-20-149

Fifteen targets were mounted along the girders of Bridge B-20-149 as shown in Figure 12. For this bridge, targets 8 and targets 10 to 13, along external Girder 8, provided its longitudinal deformed shape, while the remaining targets were distributed transversally to determine the distribution of the loads among the girders. As for the case of Bridge B-20-148, three reference points were used for triangulation.

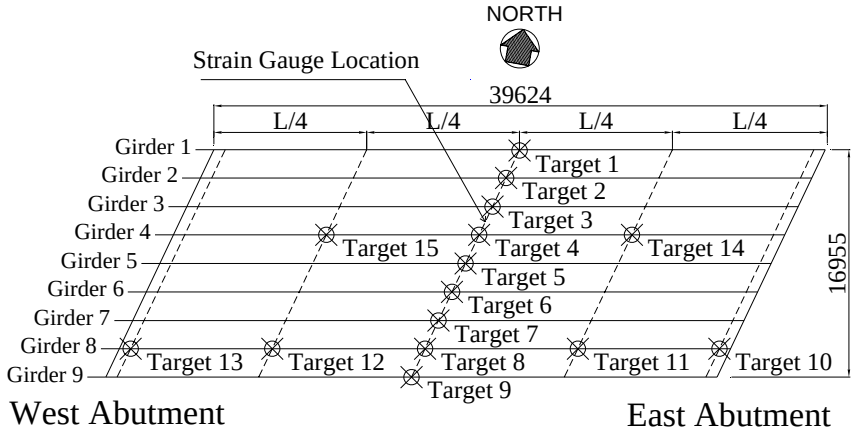

Figure 12 Target Positions of Bridge B-20-149: Plan View (Drawing not in scale)

Strain gages were installed during the construction phase of the bridge (Figure 9 and Figure 10) copying the same pattern used for Bridge B-20-148 (Conachen 2005).

For this bridge, the load test was carried out by using six fully loaded H-20 dump trucks as shown in Figure 11. All trucks were weighted before load testing and coded with a number. Table 2 summarizes the weights and load distribution between front and rear axles of the trucks used for the test. The train of trucks and the average distance between the front axle of a truck and the rear axle of the truck in front of it was 2.59 m.

Table 2 Trucks Used for Test of Bridge B-20-149

Truck Code	**Total Weight** (kN)	**Front Axle (P_1)** (kN)	**Each Rear Axle (P_2)** (kN)
1	328.0	117.6	117.6
2	321.0	107.2	107.2
3	345.2	116.7	116.7
4	324.5	108.3	108.3
5	336.5	107.8	107.8
6	330.1	118.5	118.5

2.2 Load Testing Methodology

2.2.1 Bridge B-20-148

Four load configurations identified as Test 1, 2, 3 and 4 were planned to produce maximum deflections. For tests 1 and 2, two trains of trucks (three trucks each train) were transversally placed and centered on Girders 2 and 4 (see Figure 13). This configurations were intended to produce the maximum deflection of the girders.

Test 3 and 4 were indented to produce maximum deflection of Girders 6 and 2 respectively. Details of all tests configurations are summarized in Figure 13 and Figure 14.

A “zero reading” (i.e. bridge without trucks) was taken before testing to have the benchmark and at the end of the test to determine any residual deformation. Marks were made on the asphalt to indicate the trucks test configurations following the skew of the bridge. The train of trucks for Test 1 is presented in the picture of Figure 15.

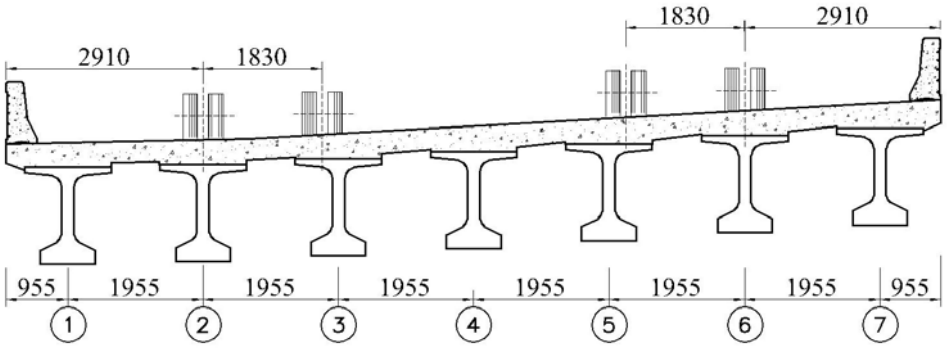

a) Test 1

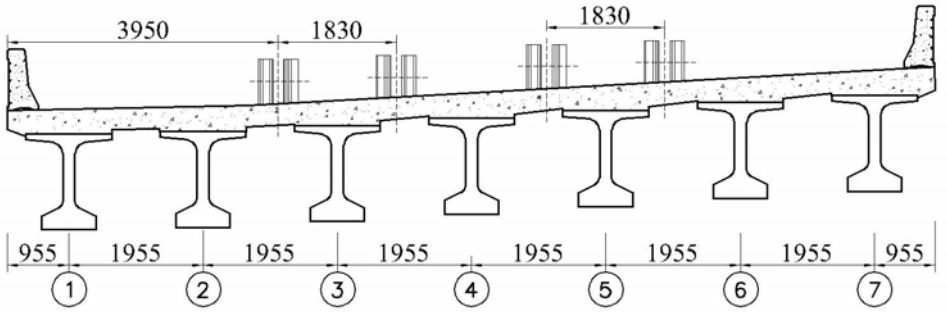

b) Test 2

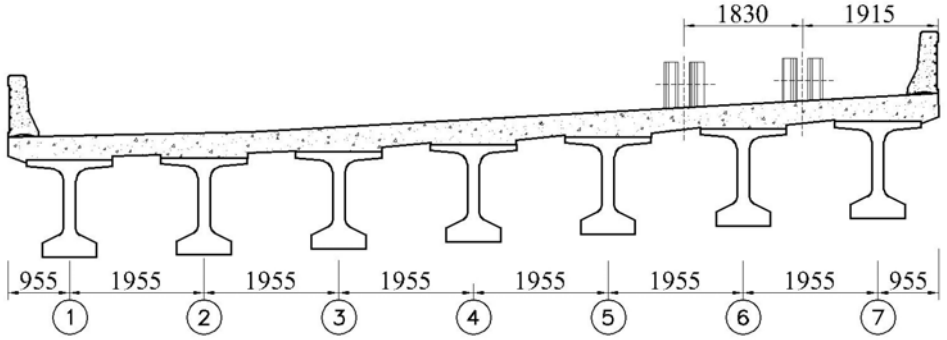

c) Test 3

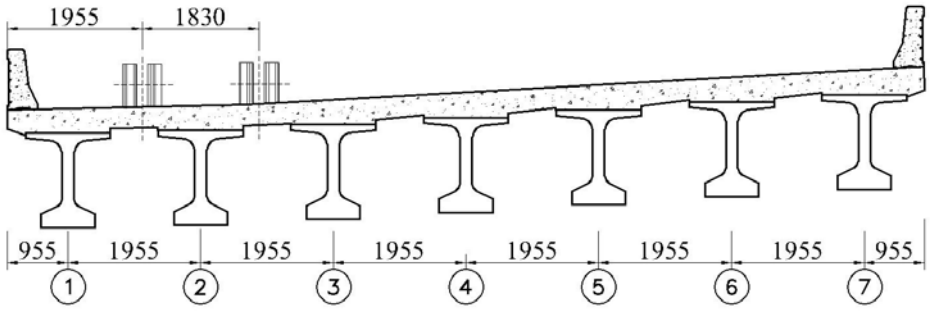

d) Test 4

Figure 13 Transversal Position of the Trucks

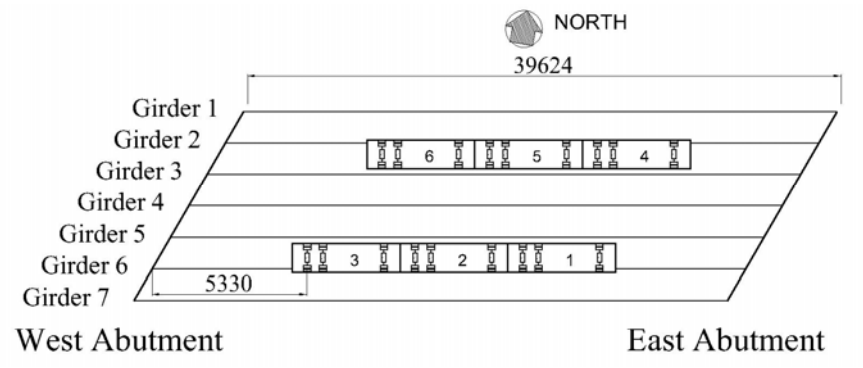

a) Test 1

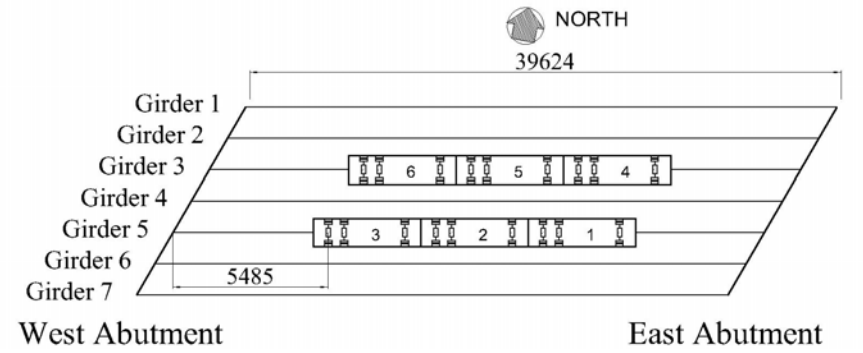

b) Test 2

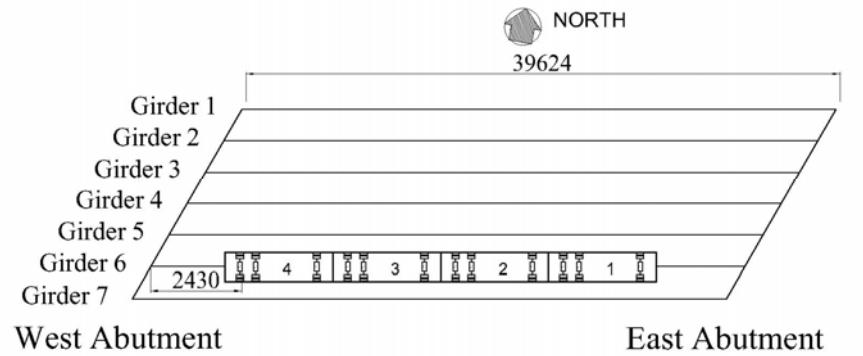

c) Test 3

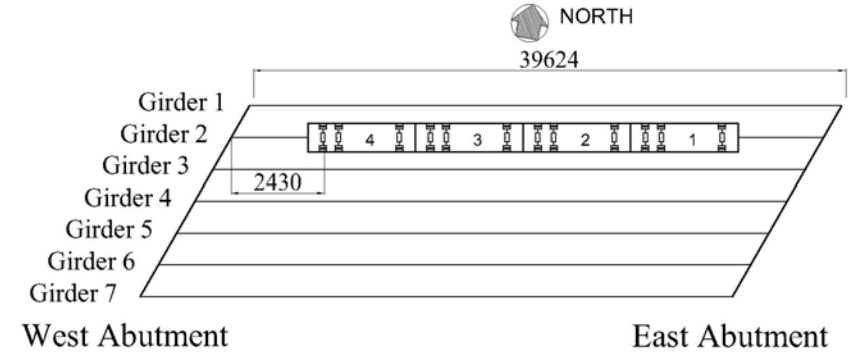

d) Test 4

Figure 14 Truck Configurations During Load Testing of Bridge B-20-148 (Drawing not to scale)

Figure 15 Trucks Aligned During Test 1

Once the total station was leveled and acclimatized, initial readings were taken for each prism. Afterwards, the trucks drove to the configuration of test 1. At each test, before acquiring data, ten minutes lapsed to allow for potential settlements. To assure stable measurements, two readings were taken for each target in order to average out errors. Once the readings were taken, the trucks moved to the next stop and the same procedure was repeated. No strain data were collected during the static tests due to equipment problems.

2.2.2 Bridge B-20-149

For this bridge, three load configurations identified as Test 1, 2 and 3 were planned to produce maximum deflections. Test 1 was intended to produce maximum deflection over Girder 8. During test 2, two trains of three trucks were transversally placed between Girders 3 and 4 and between Girders 7 and 8 to produce maximum deflection at mid-span. Test 3 was indented to produce maximum deflection of Girder 4. Details of the tests are summarized in Figure 16 and Figure 17.

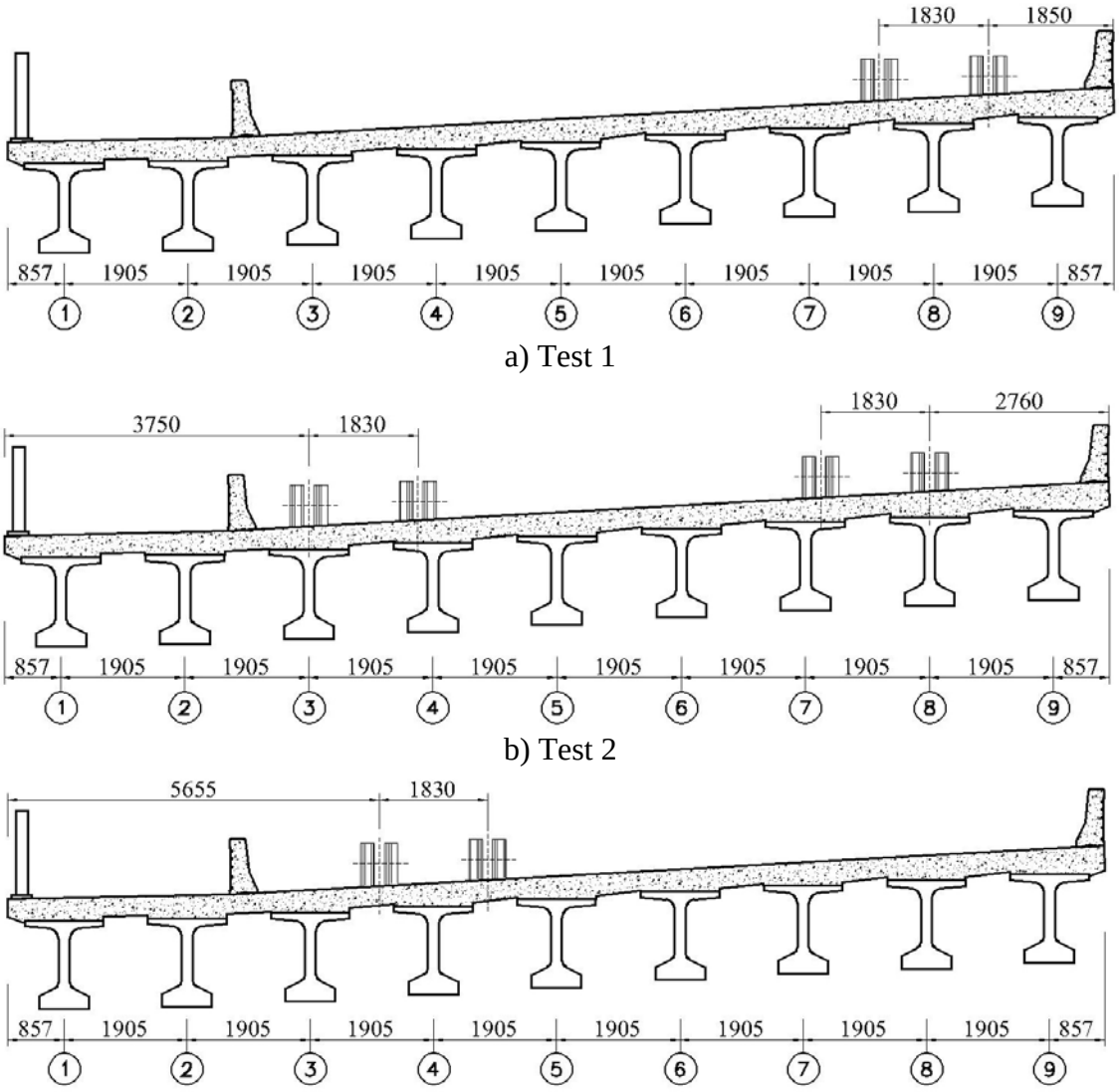

Figure 16 Transversal Position of the Trucks

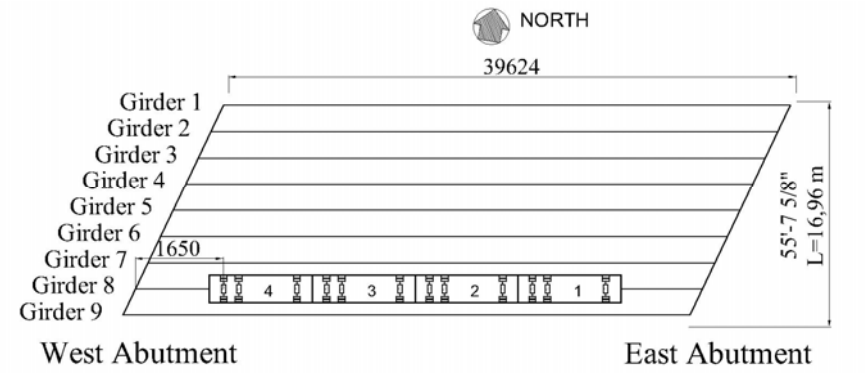

a) Test 1

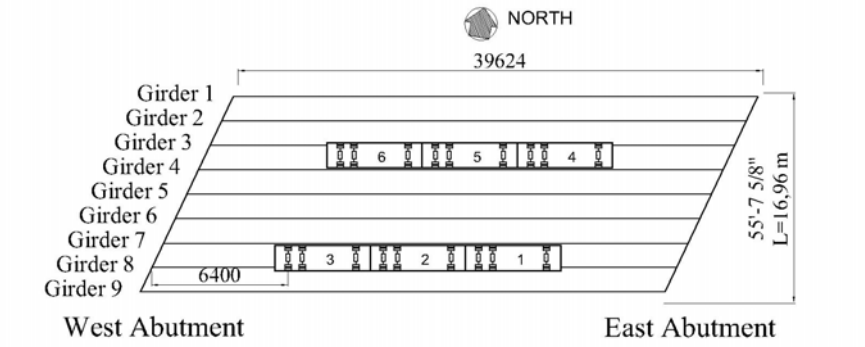

b) Test 2

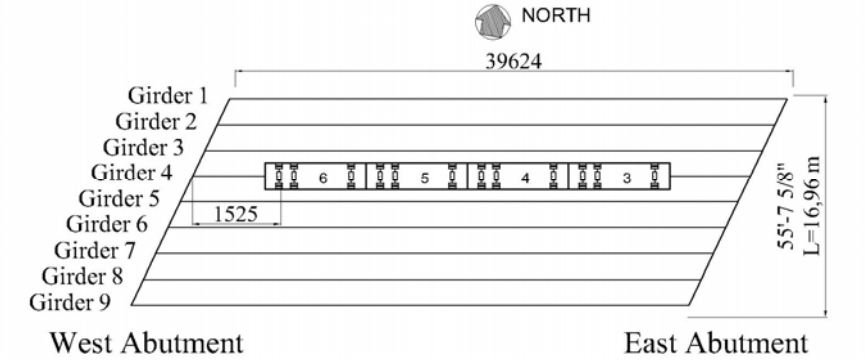

c) Test 3

Figure 17 Truck Configurations During Load Testing of Bridge B-20-149 (Drawing not to scale)

Before the test started, a “zero reading” (i.e. the bridge was not loaded) was taken to be the benchmark and at the end of the test to determine any residual deformation. Marks were made on the asphalt to indicate the trucks configuration of each test. The train of trucks for test 1 is shown in the picture of Figure 18.

Figure 18 Trucks Aligned on Test 1

2.3 Test Results

2.3.1 Bridge B-20-148

The vertical deflections resulting from the load tests are given below. Figure 19 shows the deflection of Girder 2 corresponding to four load configurations used during the test. The origin of the "z" axis in the plot of Figure 19 is located at the left support (west abutment) of Girder 2. The first point plotted in Figure 19 shows the experimental values obtained for target 12 during each test (see Figure 7). Target 12 was located at a distance equal to 0.80 m from the west abutment toward mid-span.

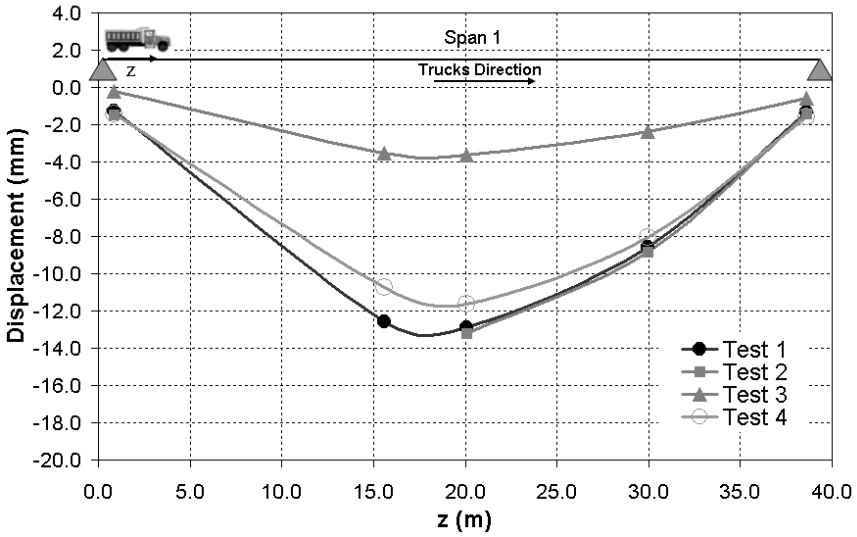

Figure 19 Longitudinal Deflections of Girder 2 Tests 1 to 4

A preliminary examination of the data indicates that the readings are accurate. The consistency of the readings from test to test gives credence to their validity. The curves also exhibit, in general, a good transition from point to point.

Figure 20 displays the transversal distribution of the girders deflections at mid-span for each test (Targets 1 through 7).

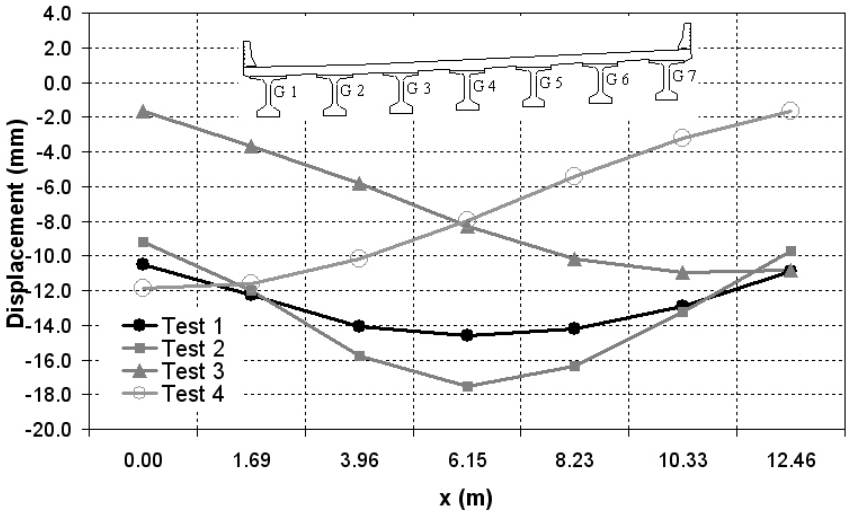

Figure 20 Vertical Deflections at L/2 from West Abutment Tests 1 to 4

Figure 21 displays the longitudinal displacement along Girder 6 during Tests 1, 2, 3 and 4. For Girder 4, the maximum value of displacement was obtained for the load configuration of test 2 and its value is approximately 18 mm. This value is lesser than the serviceability limit value recommended by the AASHTO (1998) specifications (L/800) which in this case is approximately 50 mm.

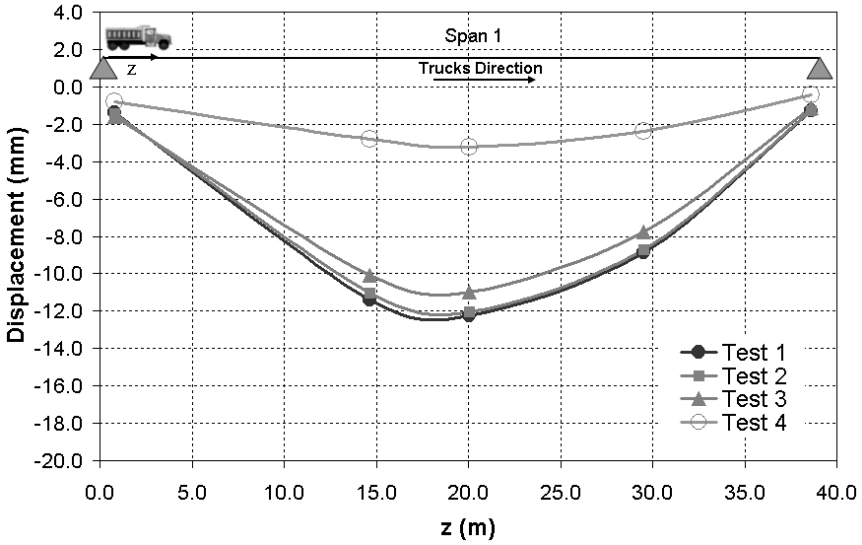

Figure 21 Longitudinal Deflections of Girder 6 Tests 1 to 4

2.3.2 Bridge B-20-149

The vertical deflections resulting from the load testing are given below. Figure 22 shows the lateral deflection of Girder 8 corresponding to each test. The curves exhibit a good transition from point to point. The origin of the "z" axis in the plot of Figure 22 is located on the west abutment (left support). The first point plotted (from left to right) shows the experimental values obtained at target 13 (see Figure 12) which 13 was located at a distance equal to 1.10 m from the west abutment toward mid-span.

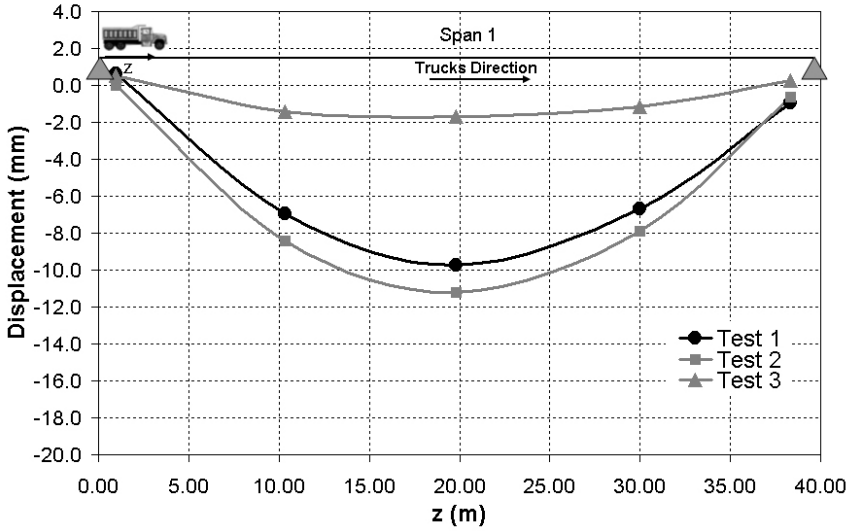

Figure 22 Longitudinal Deflections of Girder 8 Tests 1 to 3

Figure 23 displays the transversal distribution of the girders deflection at mid-span (Targets 1 through 9). The origin of the x-axis is on target 1 (first point plotted from left to right) and the distance between each target correspond to the girder spacing computed according to the north and east coordinates saved by the RTS. It can be observed that the maximum displacement of Girder 8 was obtained for Test 2 and its value is approximately 12.0 mm.

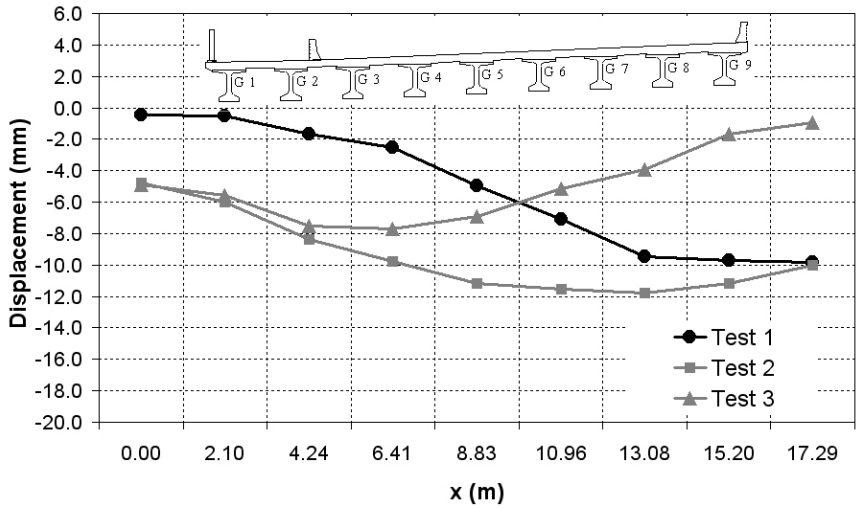

Figure 23 Vertical Deflections at L/2 from west abutment Stops 1 to 3

Figure 24 shows the longitudinal displacement along Girder 4 for the load configurations of tests 1, 2, 3 and 4. For this girder, data were collected for targets 15, 4 and 14 (Figure 12). The maximum value of displacement was obtained for the load configuration of test 2 and its value is approximately 11.5mm. This value is lesser than the serviceability limit value recommended by the AASHTO specifications (L/800) which is approximately 50 mm.

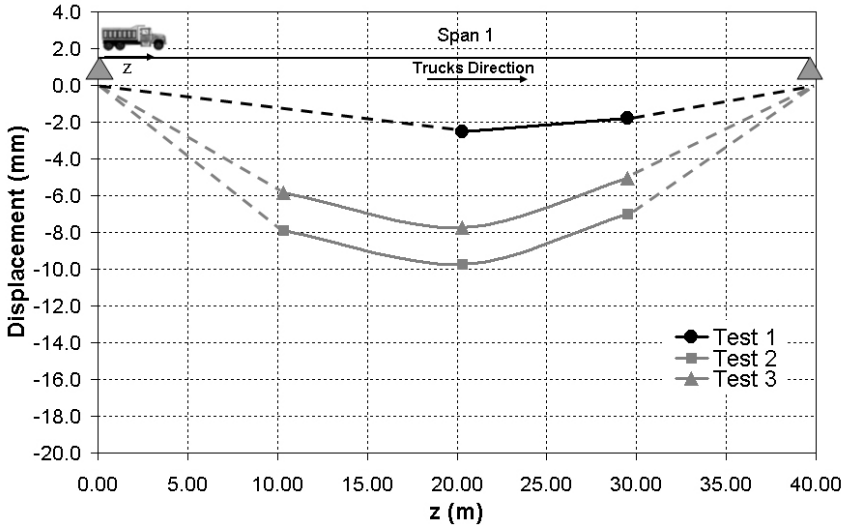

Figure 24 Longitudinal Deflections of Girder 4 Tests 1 to 3

2.4 Discussion of Results

2.4.1 Bridge B-20-148

The experimental deflections of Girder 1 were compared with the results based on a 1-D beam analysis. The girder distribution factors, GDF (defined as the ratio of the maximum moment on a girder at a given live load condition, and the maximum theoretical moment determined according to the AASHTO LRFD Bridge Design Specifications (1998) [section 4.6.2.6]. A multiple presence factor m=1 was assumed when using the lever rule. Details of calculation are summarized in Table 3 and Table 4.

Table 3 GDFs as per AASHTO LRFD Bridge Design Specifications (1998)

Girder No.	**No. of Lanes Loaded**	**AASHTO Formula**	***GDF Spans 1 and 2***
1, 7	2	$GDF_E = e.GDF_{2,4},\ e = 0.77 + \frac{d_e}{2800} = 0.997$	0.49[a]
2, 3, 4, 5, 6	2	$\mathrm{GDF_1} = \left(0.075 + \left(\frac{S}{2,900}\right)^{0.6}\left(\frac{S}{L}\right)^{0.2}\left(\frac{K_g}{L*ts^3}\right)^{0.1}\right).R_f$	0.54[a]
1, 7	1	$GDF_E.P = \left[\left(\frac{P}{2}\right)e_1 + \left(\frac{P}{2}\right)e_2\right] * \frac{1}{S}$; *(Lever rule)*	0.45[a]
2, 3, 4, 5, 6	1	$GDF_I = \left(0.06 + \left(\frac{\mathrm{S}}{4300}\right)^{0.4}\left(\frac{\mathrm{S}}{\mathrm{L}}\right)^{0.3}\left(\frac{\mathrm{K_g}}{\mathrm{L*t_s^3}}\right)^{0.1}\right).R_f$	0.38[a]

[a] See NOTATIONS for parameters and units

Table 4 Input Data for Calculations of GDFs (AASHTO, 1998)

Parameter	**Definition**	**Value**
S (mm)	Girder spacing	1955
L (mm)	Span length	39624
I (mm^4)	Moment of inertia of the concrete girder section	$1.2887*10^{11}$
E_s (MPa)	Modulus of elasticity of concrete girder	38505
E_{cs} (MPa)	Modulus of elasticity of concrete slab	29462
A (mm^2)	Cross sectional area of girder	495640
e_g (mm)	Distance between center of gravity of girder and deck	814.3
t_s (mm)	Thickness of concrete deck	200
θ deg	Skew angle	25
d_e (mm)	Distance between center of exterior girder and barrier edge	396
K_g (mm^4)	$K_g = n(I + Ae_g^2)$	$5.9797*10^{11}$
n	$n = E_s / E_{cs}$	1.307
C_1	$C_1 = 0.25\left(\frac{K_g}{Lt_s^3}\right)^{0.25}\left(\frac{S}{L}\right)^{0.5}$	0.0651
R_f	$R_f = 1 - C_1(\tan\theta)^{1.5}$	1.0

For interior girders, the width of the concrete slab section was selected as the average spacing of adjacent girders [4.6.2.6.1], *i.e.* S =1955 mm.

Figure 25 shows a comparison between the experimental deflections of Girders 2 and 6 and their analytical deformed shapes. The deflections measured through the RTS system are generally smaller than the theoretical values, and clearly bellow the L/800 limit of 50 mm [2.5.2.6.2], as shown in Figure 25, thereby demonstrating that serviceability of the bridge is below the AASHTO computed value.

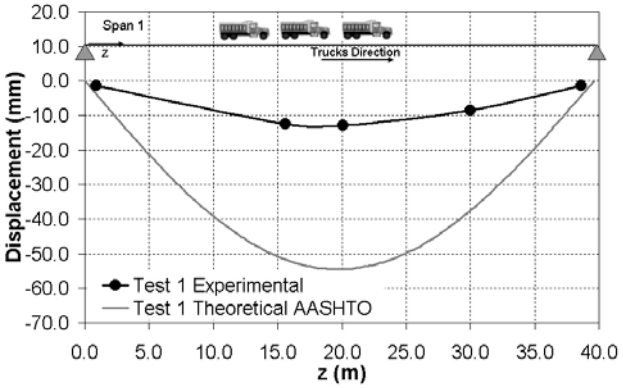

a) Test 1 (Girder 2)

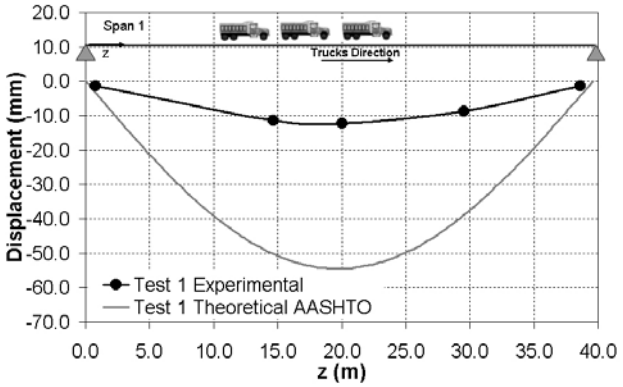

b) Test 1 (Girder 6)

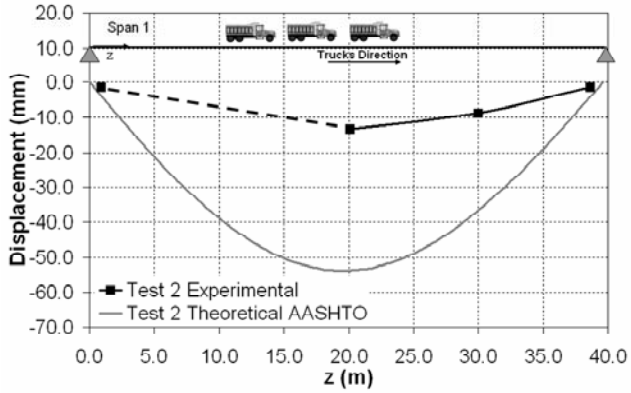

c) Test 2 (Girder 2)

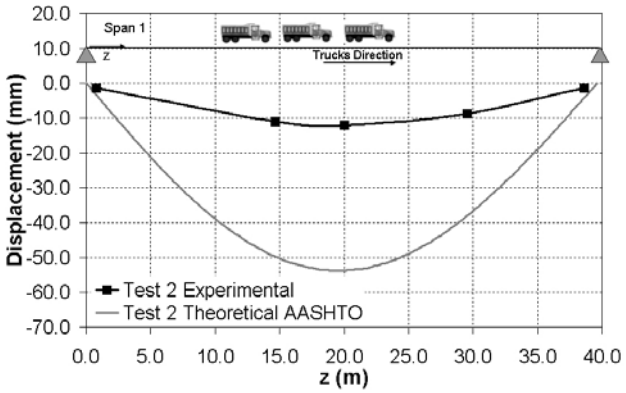

d) Test 2 (Girder 6)

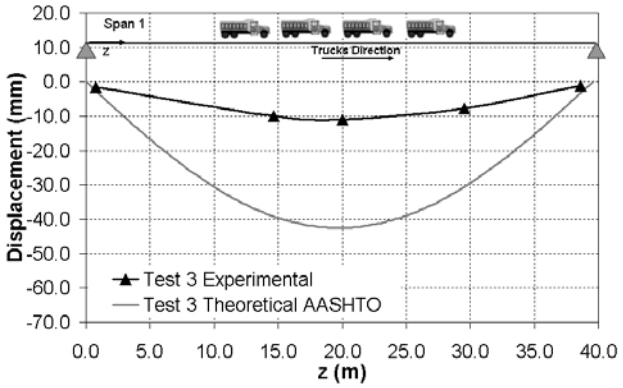

e) Test 3 (Girder 6)

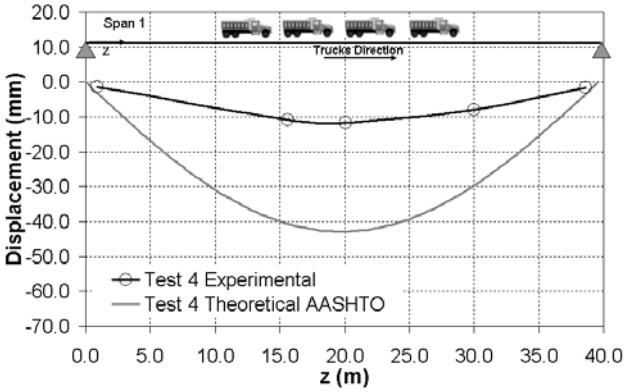

f) Test 4 (Girder 2)

Figure 25 Comparison Between AASTHO Provisions and Experimental Results

The GDF for the *i*th girder at mid-span was estimated from the deflection data retrieved as:

$$\mathrm{GDF}_i = \frac{\delta_i}{\sum_{j=1}^{n} \delta_j} \qquad (1)$$

Wherein, δ_i is representing the deflection of the ith girder. In case of Bridge B-20-148, *n* is equal to 7 and for bridge B-20-149 *n* is equal to 9. Figure 26 and Figure 27 show the GDFs calculated for each test taking into account if the load configuration corresponds to one or two loaded lanes. The curves that correspond to the GDF of the test were computed by using Eq. (1). Moreover, Figure 26 and Figure 27 allow evaluate the safety factor of the GDF proposed by AASHTO.

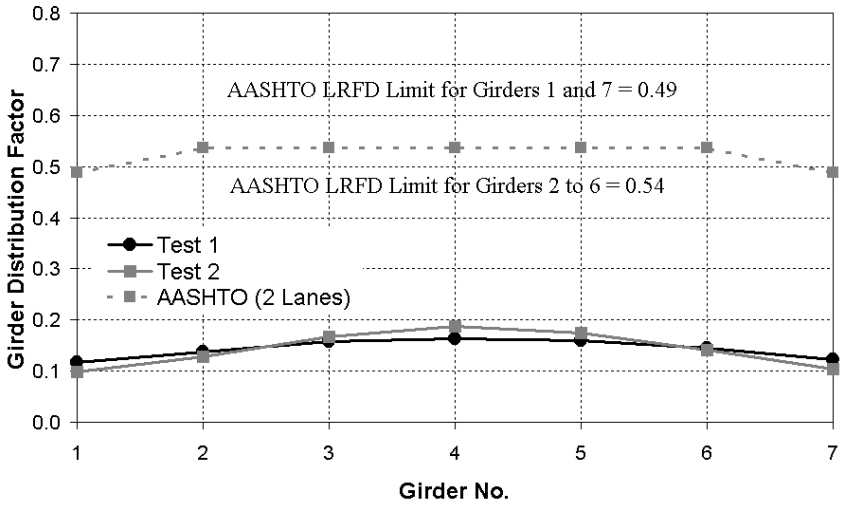

Figure 26 Comparison Between AASHTO and Experimental GDF at Mid-span (Two Lanes Loaded, Tests 1 and 2)

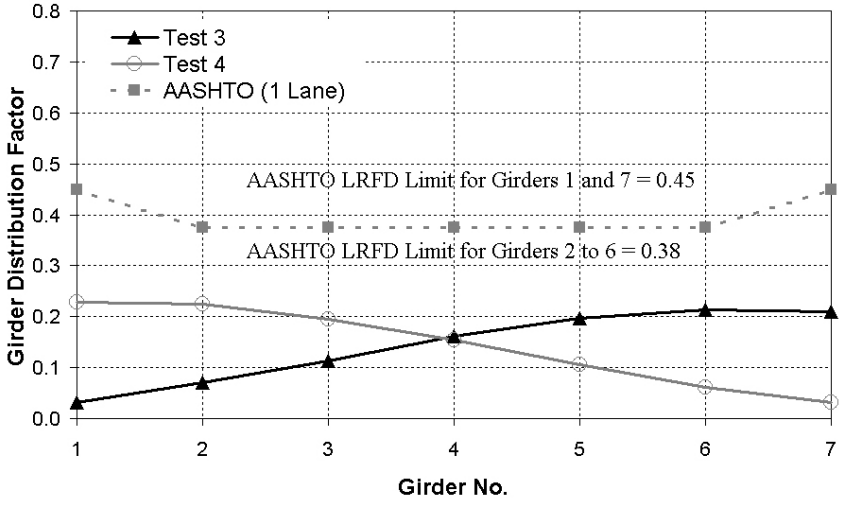

Figure 27 Comparison Between AASHTO and Experimental GDF at Mid-span (One Lane Loaded, Tests 3 and 4)

The safety factor was computed as the ratio between the analytical GDF proposed by AASHTO and the test GDF obtained by Eq. (1). The minimum safety factor (Girder 4) is equal to 2.84 for

the case of two-loaded lanes (Tests 1 and 2) and 1.72 (Girder 1) for the case of one-loaded lane (Test 3 and 4).

2.4.2 Bridge B-20-149

The experimental deflections of Girders 4 and 8 were compared to the results based on a 1-D beam analysis. The GDFs were determined according to the AASHTO LRFD Bridge Design Specifications (1998) [section 4.6.2.6]. Details of calculation are summarized in Table 5 and Table 6. For interior girders, the width of the concrete slab section was selected as the average spacing of adjacent girders [4.6.2.6.1], *i.e.* S = 1905 mm. The width of the concrete slab section was selected as 200 mm.

Table 5 GDFs as per AASHTO LRFD Bridge Design Specifications (1998)

Girder No.	**No. of Lanes Loaded**	**AASHTO Formula**	***GDF Spans 1 and 2***
1, 9	2	$GDF_E = e.GDF_{2,4},\ e = 0.77 + \frac{d_e}{2800} = 0.997$	0.46[a]
2-8	2	$\mathrm{GDF_I} = \left(0.075 + \left(\frac{S}{2{,}900}\right)^{0.6}\left(\frac{S}{L}\right)^{0.2}\left(\frac{K_g}{L*ts^3}\right)^{0.1}\right).R_f$	0.52[a]
1, 9	1	$GDF_E.P = \left[\left(\frac{P}{2}\right)e_1 + \left(\frac{P}{2}\right)e_2\right] * \frac{1}{S}$; *(Lever rule)*	0.42[a]
2-8	1	$GDF_I = \left(0.06 + \left(\frac{\mathrm{S}}{4300}\right)^{0.4}\left(\frac{\mathrm{S}}{\mathrm{L}}\right)^{0.3}\left(\frac{\mathrm{K_g}}{\mathrm{L*t_s^3}}\right)^{0.1}\right).R_f$	0.37[a]

[a] See NOTATIONS for parameters and units

Table 6 Input Data for Calculations of GDFs (AASHTO, 1998)

Parameter	**Definition**	**Value**
S (mm)	Girder spacing	1905
L (mm)	Span length	39624
I (mm^4)	Moment of inertia of the concrete girder section	$1.2887*10^{11}$
E_s (MPa)	Modulus of elasticity of concrete girder	37138.0
E_{cs} (MPa)	Modulus of elasticity of concrete slab	30995.0
A (mm^2)	Cross sectional area of girder	495640
e_g (mm)	Distance between center of gravity of girder and deck	814.3
t_s (mm)	Thickness of concrete deck	200
θ deg	Skew angle	25
d_e (mm)	Distance between center of exterior girder and barrier edge	300
K_g (mm^4)	$K_g = n(I + Ae_g^2)$	$5.482*10^{11}$
n	$n = E_s / E_{cs}$	1.198
C_1	$C_1 = 0.25\left(\frac{K_g}{Lt_s^3}\right)^{0.25}\left(\frac{S}{L}\right)^{0.5}$	0.0629
R_f	$R_f = 1 - C_1(\tan\theta)^{1.5}$	1.0

Figure 28 shows a comparison between the experimental deflections at girders 4 and 8 and their analytical deformed shapes. The deflections measured through the RTS system are generally smaller than the theoretical values, and clearly bellow the L/800 limit of 50 mm [2.5.2.6.2], as shown in Figure 28, thereby demonstrating that serviceability of the bridge is below the AASHTO computed value

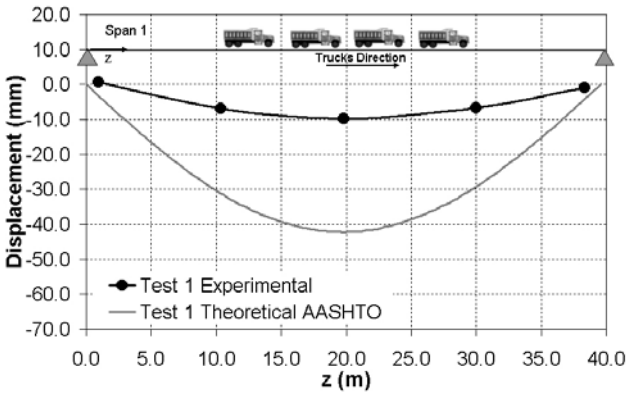

a) Test 1 (Girder 8)

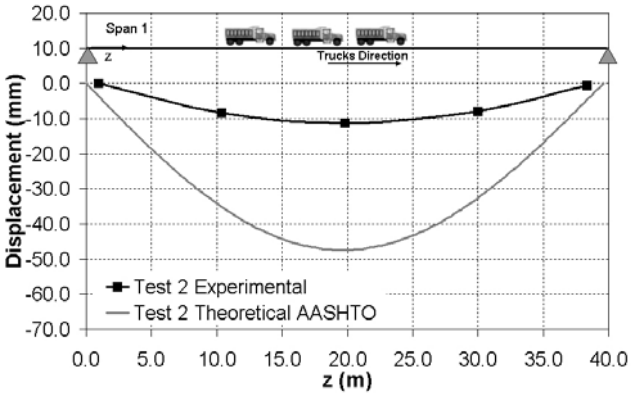

b) Test 2 (Girder 8)

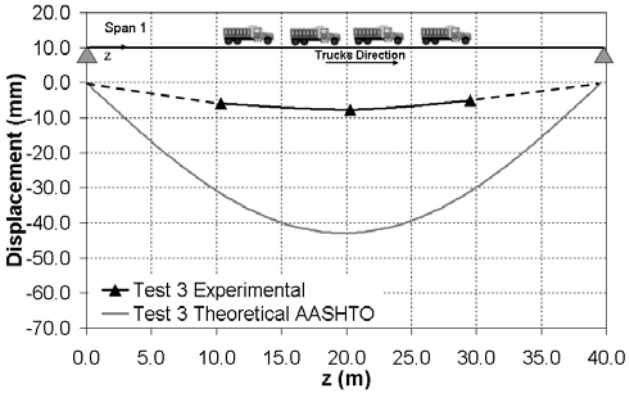

c) Test 3 (Girder 4)

Figure 28 Comparison Between AASTHO Provisions and Experimental Results

The GDF for the *i*th girder at mid-span was estimated from the deflection data recorded during the load test and by using Equation (1). Figure 29 and Figure 30 show the girder distribution factors computed at each test taking into account one or two loaded lanes.

The safety factor was calculated as per bridge B-20-148. The minimum safety factor (Girder 7) is equal to 3.70 for the case of two-loaded lanes (Tests 2). The minimum safety factor (Girder 8) for the case of one-loaded lane (Test 1 and 2) is equal to 1.76.

For both bridges, the values of GDFs determined experimentally at mid-span are always below those based on the AASHTO provisions, which are proven conservative. One reason for this difference is that the transverse stiffening action of the parapets is neglected by the design formulas wherein the thickness of the deck is the only parameter that explicitly accounts for a degree of transverse stiffness in the structural system.

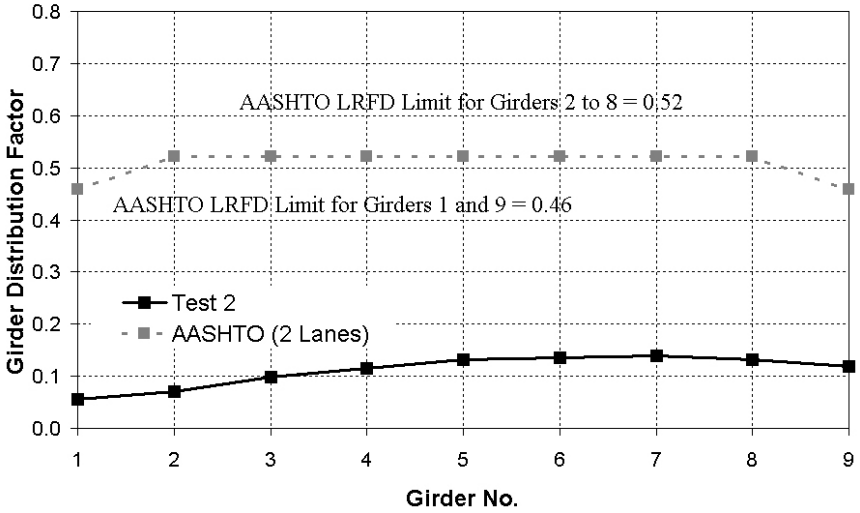

Figure 29 Comparison Between AASHTO and Experimental GDF at Mid-span (Two Lanes Loaded, Test 2)

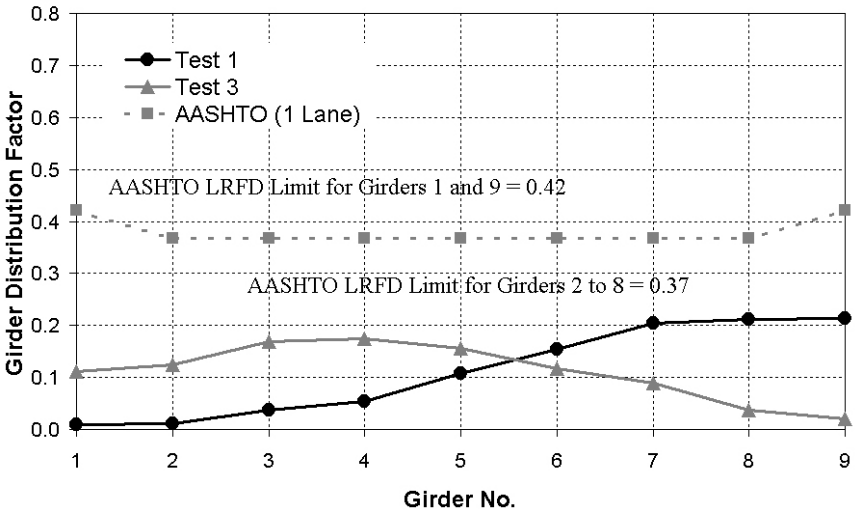

Figure 30 Comparison Between AASHTO and Experimental GDF at Mid-span (One Lane Loaded, Test 1 and 3)

2.5 Finite Element Method Simulations

FEM simulations were created based upon the data obtained from the diagnostic test. These numerical models may be used to approximate the bridges' behavior to limiting loads. A three-dimensional model of the main structural elements was used. The model consisted of 3-D solid elements that represented the deck, girders and parapets acting as a composite structure. The spacing used between the girders was the same as the one of each actual bridge. For a truck placed anywhere on the deck, the mesh allowed accurate transverse distribution of wheel loads to the girders. A depiction of the Finite-Element meshes used for each bridge are shown in Figure 31 and Figure 32.

The FEM Models were implemented by using the commercial software Abaqus 6.4. A linear elastic analysis was performed for each of the load configurations of each bridge.

The Finite Element used for the simulations was the so-called “C3D8” which is a continuum (solid) 3-D element that has eight nodes with three active degrees of freedom (DOF) per node. The active degrees of freedom are the translations along each of the global coordinate axis (x, y and z-axis).

The contribution of the rail guard was taken into account in the FEM Model by modeling them with representative rectangular sections that have equivalent area and inertia. In order to consider the difference of the stiffness of the concrete elements that constitute the bridge structure (girders, deck and parapets), two different materials were defined in the FEM Model of each bridge.

For bridge B-20-148, the concrete of the deck and parapets was modeled as having an f’c equal to 39 MPa (5620 psi), while the concrete of the girders was modeled with a f’c equal to 66 MPa (9600 psi).

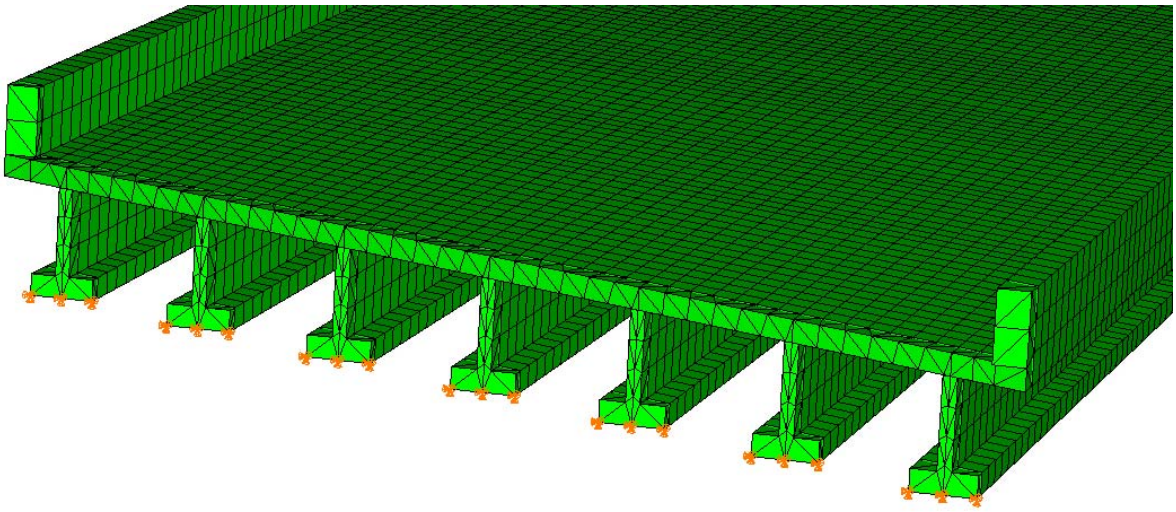

Figure 31 Finite Element Model of Bridge B-20-148

In the case of bridge B-20-149, the concrete of the deck and parapets was taken into account as having a f’c equal to 43 MPa (6220 psi) and the concrete of the girders was modeled with a f’c equal to 61.5 MPa (8930 psi).

The effect of the diaphragms was not implemented in the FEM Model. Figure 31 and Figure 32 show a detail of the mesh at left support (west abutment) of each bridge. The supports (west and east abutments) were modeled as fixed supports (three DOF restricted). The loads of the trucks were applied as concentrated loads at nodes that coincided with the location of the truck wheels during the tests.

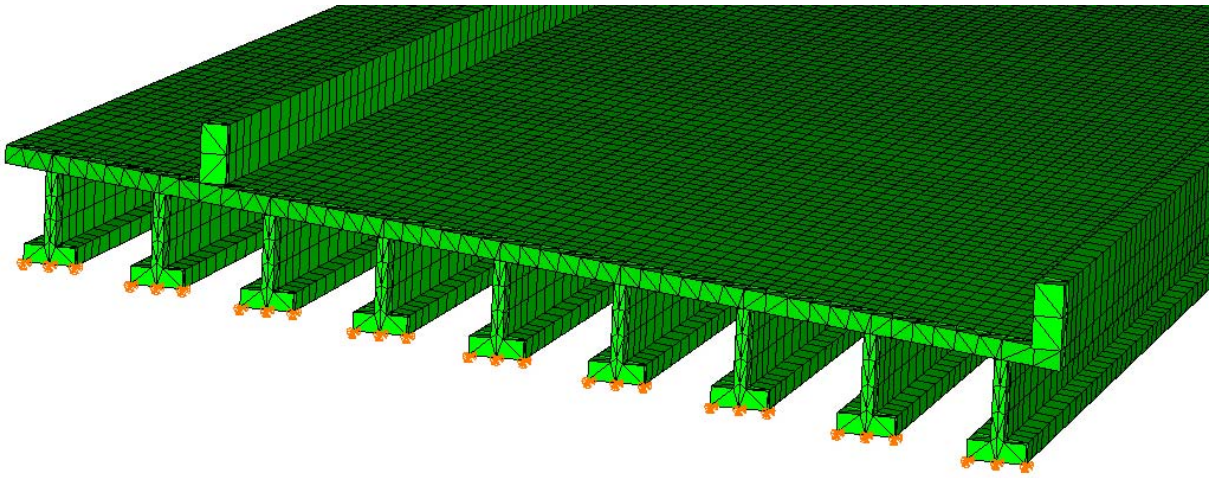

Figure 32 Finite Element Model of Bridge B-20-149

2.5.1 Bridge B-20-148

Figure 33 compares the FEM Model results to those directly measured in the field during Tests 1 through 4 of bridge B-20-148. The results correspond to the measurements of Girder 6. The numerical model was found to be adequately accurate describing the longitudinal deflections measured in the field.

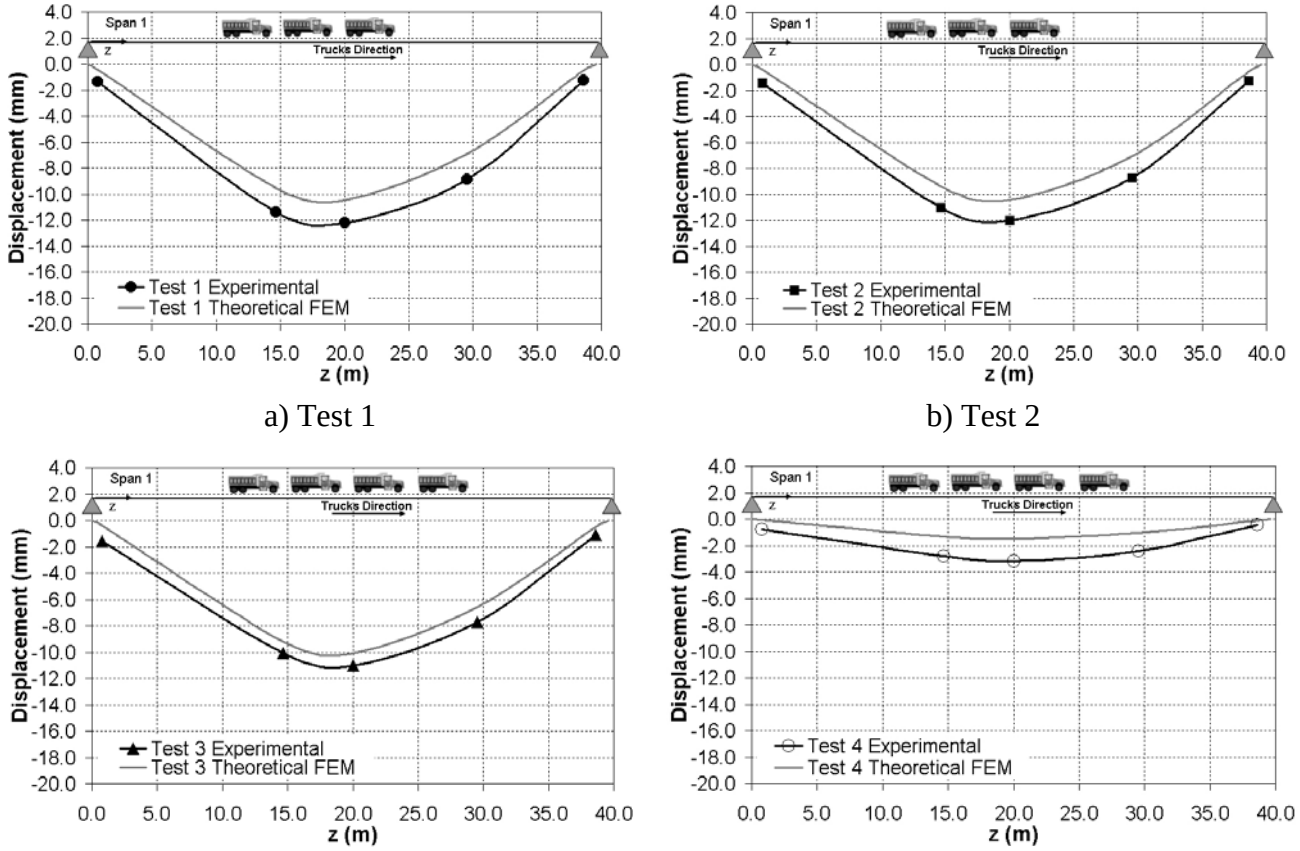

a) Test 1

b) Test 2

c) Test 3

d) Test 4

Figure 33 Comparison between FEM Model and Experimental Results (Test 1 to 4)

The vertical deflections at mid-span for all the girders are compared in Figure 34. For this bridge, the model showed its effectiveness predicting transversal experimental distribution of deflections.

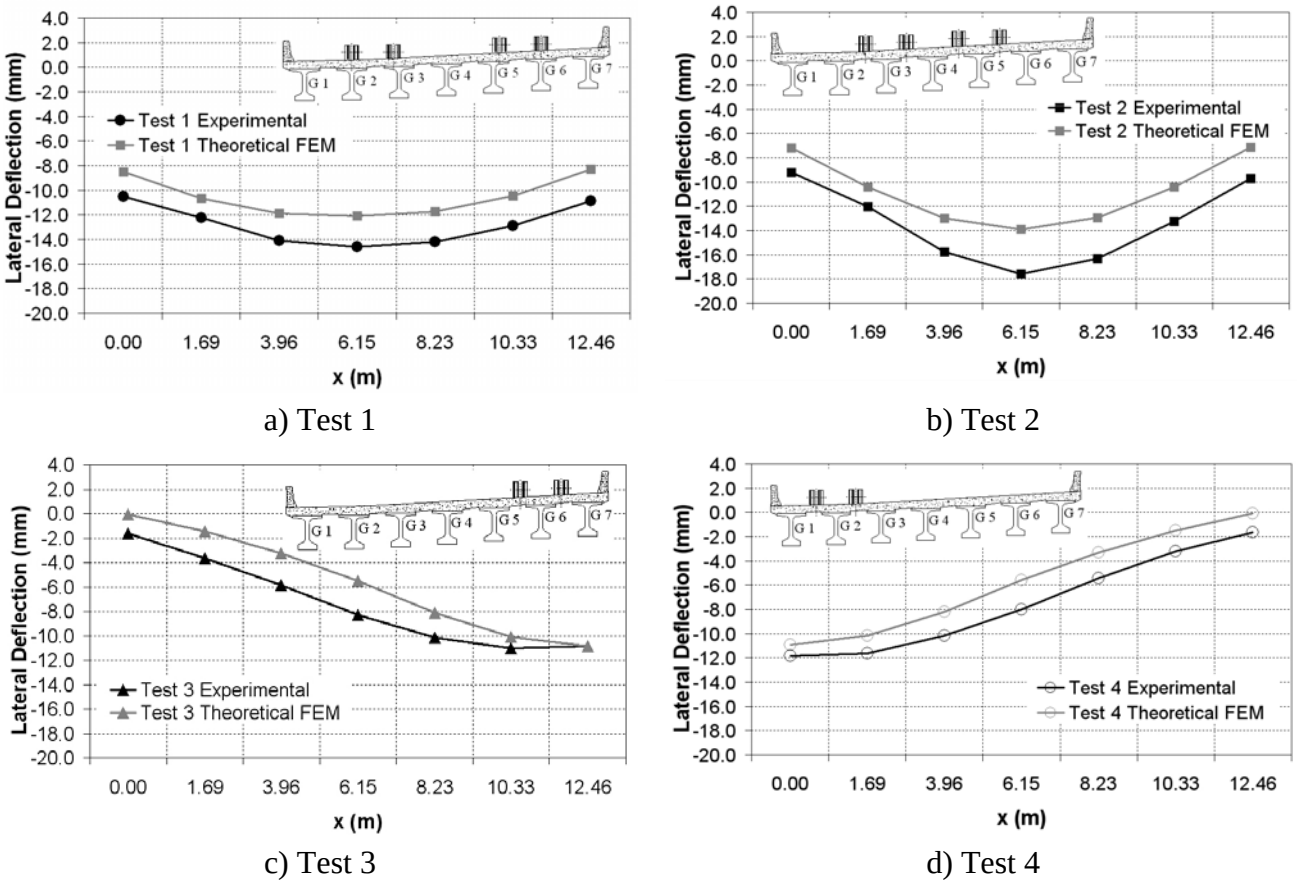

a) Test 1

b) Test 2

c) Test 3

d) Test 4

Figure 34 Comparison between FEM Model and Experimental Results (Vertical Deflections at Mid-span, Tests 1 to 4)

Figure 35 shows the strain gage readings acquired during the test. For all tests, the maximum strains in the reinforcement are below the yield limit. For this bridge, the location of the gages relative to the trucks was appropriate and the results obtained by the FEM model are representative of the strains obtained during the test. Figure 36 shows contour plots of the strains in the direction of the longitudinal FRP reinforcement of the deck for all the test configurations.

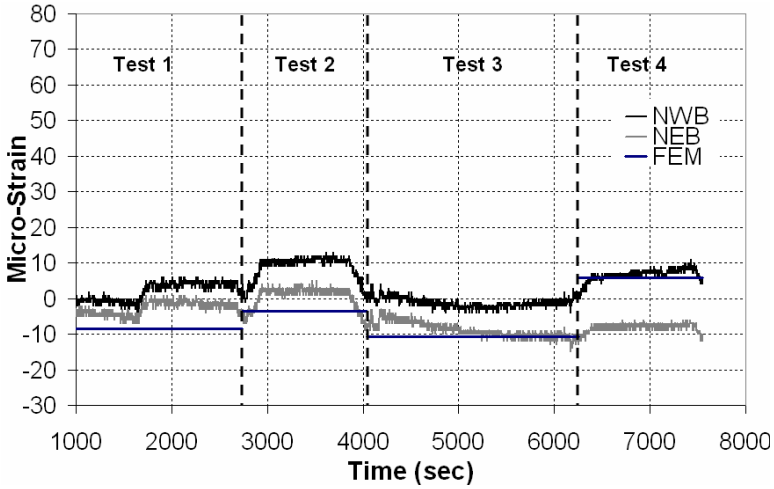

a) Gages NWB and NEB (see Figure 10)

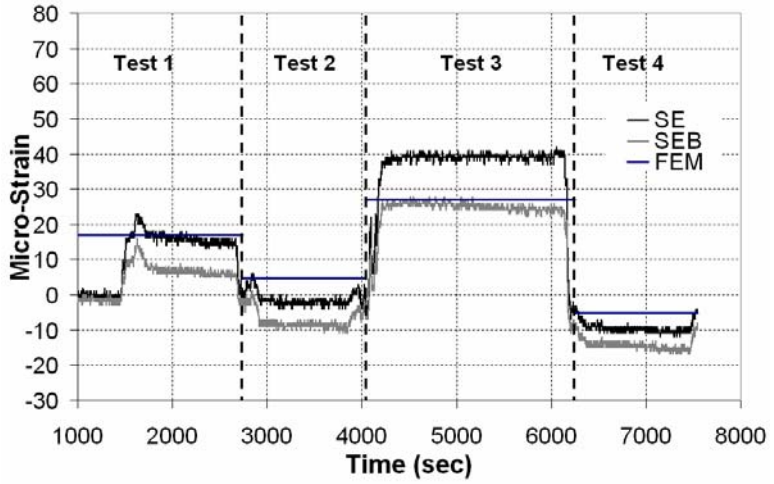

b) gages SE and SEB (see Figure 10)

Figure 35 Comparison Between Strain Gage Readings and FEM and Results

Table 7 and Table 8 summarize the values of the strain gage readings collected during the static tests and the results obtained with the FEM model simulations. The FEM results demonstrate the effectiveness of the model in also predicting strains and stresses. The computed stress values for these levels of deformations are below the FRP allowable stress.

Table 7 Comparison between Test and FEM Results (Strain Gages NWB and NEB)

Test	Strains (με)			Elastic Modulus * (ksi)**	Computed Stress (ksi)			Allowable Stress (ksi) **
	NWB	NEB	FEM		NWB	NEB	FEM	
1	5.0	-3.0	-8.5	4,500	0.023	-0.014	-0.038	80
2	11.0	3.0	-3.5	4,500	0.050	0.014	-0.016	80
3	-4.0	-11.0	-10.7	4,500	-0.018	-0.050	-0.048	80
4	7.0	-7.0	5.8	4,500	0.032	-0.032	0.026	80

Table 8 Comparison between Test and FEM Results (Strain Gages SE and SEB)

Test	Strains (με)			Elastic Modulus * (ksi)**	Computed Stress (ksi)			Allowable Stress (ksi) **
	SE	SEB	FEM		NWB	NEB	FEM	
1	16.0	9.0	17.0	4,500	0.072	0.041	0.077	80
2	-2.0	-8.0	4.7	4,500	-0.009	-0.036	0.021	80
3	42.0	28.0	27.1	4,500	0.189	0.126	0.122	80
4	-3.0	-8.0	-5.1	4,500	-0.014	-0.036	-0.023	80

* Conachen 2005
** Specification values

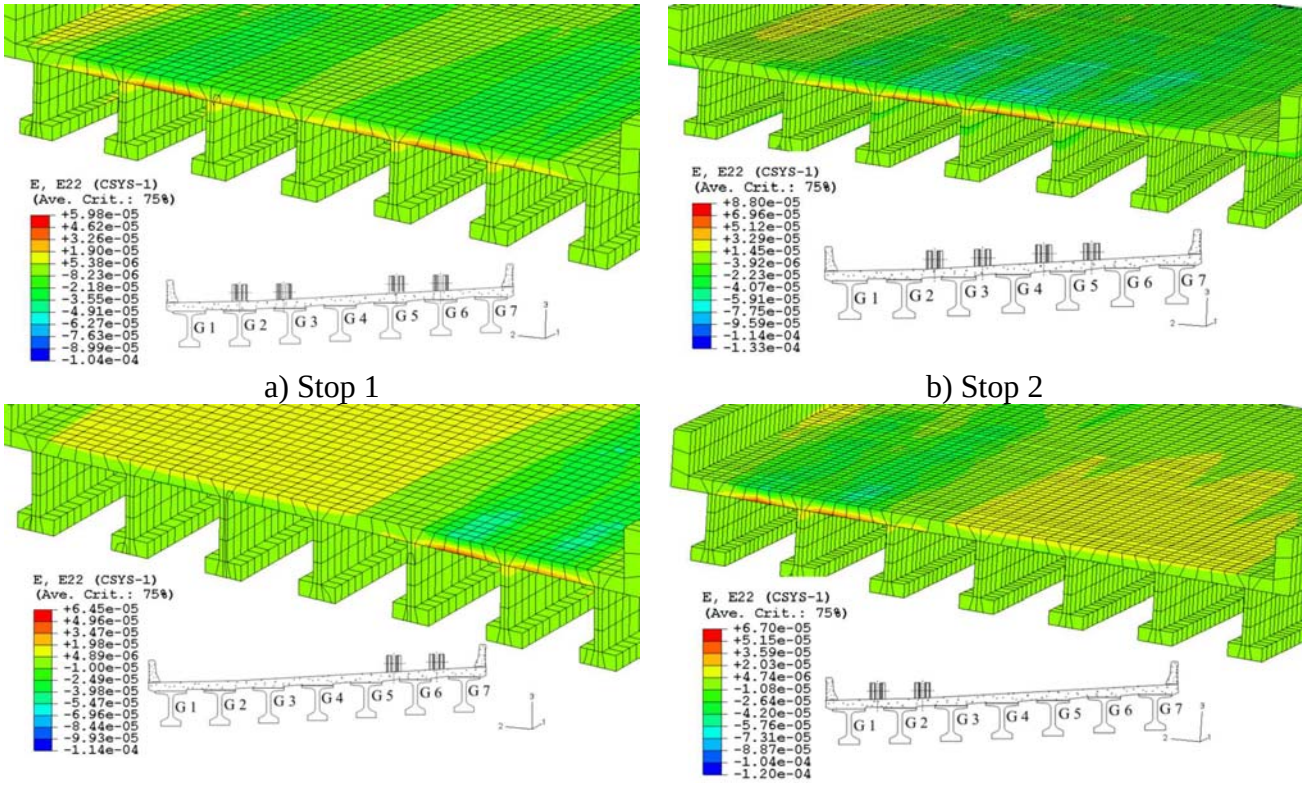

a) Stop 1 b) Stop 2

c) Stop 3 d) Stop 4

Figure 36 Plot Contour of Strain ε_{22} (Direction of the Deck Longitudinal FRP Reinforcement)

2.5.2 Bridge B-20-149

Figure 37 compares the FEM results of the internal Girder 8 to those directly measured in the field for the load configurations of the tests 1 to 3. The numerical model was found to be adequately accurate describing the longitudinal deflections measured in the field.

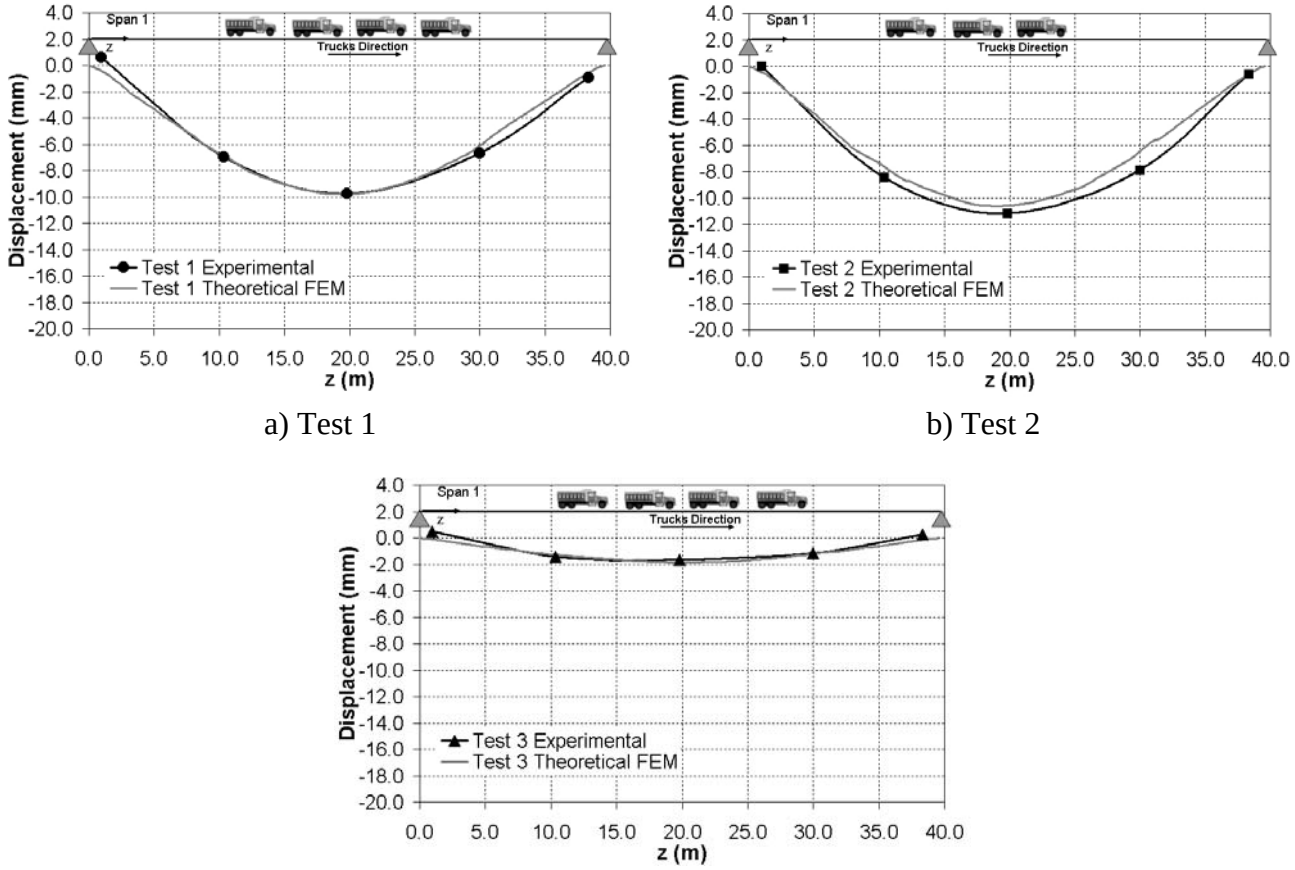

a) Test 1

b) Test 2

c) Test 3

Figure 37 Comparison between FEM Model and Experimental Results (Stops 1 to 3)

Figure 38 compares the vertical deflections computed by the FEM Model to the experimental ones. The results indicate that the model also showed its effectiveness predicting transversal experimental distribution of deflections for bridge B-20-149.

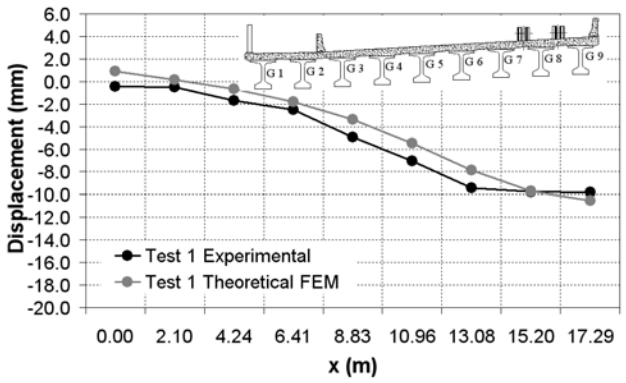

a) Test 1

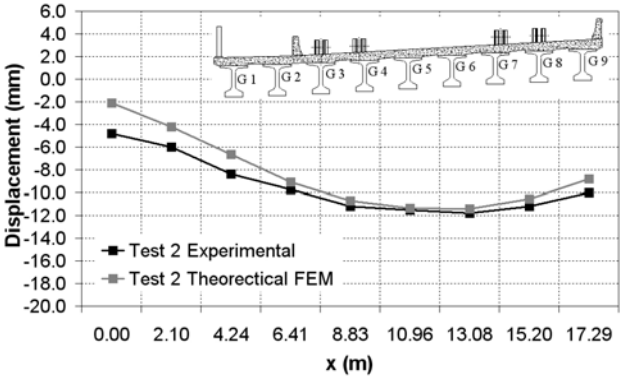

b) Test 2

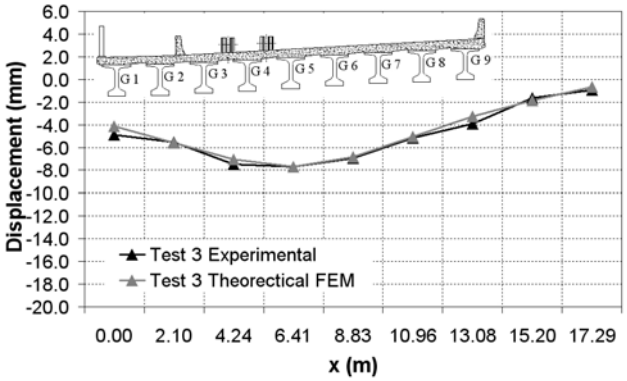

c) Test 3

Figure 38 Comparison between FEM Model and Experimental Results (Vertical Deflections at Mid-span, Tests 1 to 3)

3 SUMMARY AND CONCLUSIONS

Conclusions based on the deflection and strain measurements via Robotic Tacheometry System (RTS) and Data Acquisition System (DAS) respectively during the diagnostic load test and the comparison to analytical results based on the AASHTO LRFD Bridge Design Specifications (1998) and the numerical results based on the FEM simulations of both bridges can be summarized as follows:

- The structural assessment confirms a good response of the bridges for the serviceability, since the experimental deflections were found to be smaller than the theoretical values determined according to the design provisions (AASHTO, 1998).
- The transversal deflection distribution computed according to the AASHTO provisions diverges from the actual transversal distribution of the bridge yielding to a safe design that does not predict or evaluate the actual load carrying capacity of the structure.
- In order to obtain a benchmark for the long term monitoring of the bridges B-20-148 and B-20-149, a load test was conducted. Girder deflections and strain gage data were recorded for different truck stops configurations.
- The use of the RTS confirms its cost-effectiveness for deflection measurement. The fact that the technology allows for non-contact measurement significantly enhances its versatility.
- The deflection data collected with the RTS indicates that the readings were accurate and the consistency of the readings gives credence to their validity.
- The experimental strain data obtained for bridge B-20-148 with the DAS are useful to determine the safety of the structure since the readings obtained at the FRP reinforcement are representative of the load test configurations.
- A Finite Element model was developed. The model was able to represent the actual behavior of the bridge and can be used to determine the actual load rating of the bridges and therefore their safety over time.
- The results of the FEM analysis confirmed that the assumption of composite action between deck and girders is adequate to describe the response of the bridge during the load test.

In the future, if another load test is conducted, special attention should be given to monitoring the degradation of any constituent of the bridge to determine the actual load rating of the structure.

4 REFERENCES

American Association of State Highway and Transportation Officials (AASHTO), (1996): ‘‘LRFD standard specifications.’’ 16th Ed., Washington, D.C.

American Association of State Highway and Transportation Officials (AASHTO), (1998): ‘‘LRFD bridge design specifications.’’ 2nd Ed., Washington, D.C.

American Association of State Highway and Transportation Officials (AASHTO), (2002): “Standard Specifications for Highway Bridges”, 17th Edition, Published by the American Association of State Highway and Transportation Officials, Washington D.C.

American Concrete Institute (2005), “Guide for the Design and Construction of Concrete Reinforced with FRP Bars,” ACI 440.1R-05, American Concrete Institute, Farmington Hills, MI.

Bank, L.C., Oliva, M.G., Russel, J.S., Dieter, D.A., Dietsche, J.S., Berg, A.C., Ehmke, F.G., “Bridge B-20-133 on U.S. 151 with Fiber Reinforced Polymer Reinforced Concrete Deck”. Final Report. University of Wisconsin-Madison, January 2005.

Bank, L., Oliva, M., Russell, J., Jacobson, D., Conachen, M., Nelson, B., and McMonigal, D. (2004), “Super-Sized Double-Layer Pultruded Gratings,” COMPOSITES 2004 Convention and Trade Show, American Composites Manufacturers Association (ACMA), Oct. 6-8, 2004, Tampa, FL, CD-ROM.

Bank, L.C., and Xi, Z. (1993), “Pultruded FRP Grating Reinforced Concrete Slabs,” Fiber-Reinforced-Plastic for Concrete Structures - International Symposium (eds. A. Nanni and C.W. Dolan), SP-138, American Concrete Institute, Farmington Hills, MI, 561-583.

Bank, L.C., and Xi, Z. (1995), “Punching Shear Behavior of Pultruded FRP Grating Reinforced Concrete Slabs,” Non-metallic (FRP) Reinforcement for Concrete Structures (ed. L. Taerwe), RILEM Proceedings 29, E&FN Spon, London, 360-367.

Bank, L.C., Xi, Z., and Munley, E. (1992), “Performance of Doubly-Reinforced Pultruded Grating/Concrete Slabs,” Proceedings of the 1st International Conference for Advanced Composite Materials in Bridges and Structures (eds. K.W. Neale and P. Labossiere), October 6 9, Sherbrooke, Canada, Canadian Society for Civil Engi-neering, 351 360.

Barker, M. G., and Schrage, S. D. (2000): ‘‘High performance steel: design and cost comparisons.’’ Modern Steel Constr., 16, 35–41.

Barth, K. E., Roeder, C. W., Christopher, R. A., and Wu, H. (2004): ‘‘Evaluation of live load deflection criteria for I-shaped steel bridge design girders.’’ Proc., Int. Conf. on High Performance Materials in Bridges, Kona, Hawaii, ASCE, Reston, Va.

Bradberry, T.E. (2001), “Fiber-reinforced-plastic Bar Reinforced Concrete Bridge Decks,” Proceedings of the 80th Annual Transportation Research Board Meeting, Jan. 9-13, 2001, Washington, DC, CD #01-3247.

Berg, A. (2004). “Analysis of a bridge deck built on U.S. Highway 151 with FRP Stay-in-Place Forms, Grids, and Rebars”, Master Thesis, University of Wisconsin-Madison, 2004.

Conachen, M. (2005). “Modular 3-D FRP Reinforcing System for a Bridge Deck in Fond du Lac, Wisconsin”, Master Thesis, University of Wisconsin-Madison, 2005.

Buth, C.E., Williams, W.F., Bligh, R.P., Menges, W.L., and Haug, R.R. (2003), “Performance of the TxDOT T202 (MOD) Bridge Rail Reinforced with Fiber Reinforced Polymer Bars,” TTI Research Report 0-4138-3, Texas Transportation Institute, College Station, TX.

Casadei, P. and Nanni, A. (2003); “In-Situ Load Testing of Reinforced Concrete Structures: Case Studies”, *South East Asia Construction*, Sept/Oct 2003.

Chajes, M. J., Mertz, D. R., and Commander, B., (1997): “Experimental Load Rating of a Posted Bridge”, *Journal of Bridge Engineering*, Vol. 2, No. 1, February 1997, pp. 1-10

Clingenpeel, B. F., and Barth, K. E. (2003). ‘‘Design optimization study of a three-span continuous bridge using HPS70W,’’ AISC Eng. J., 39(3), 121–126.

El-Salakawy, E., Benmokrane, B., Masmoudi, R., Brière, F. and Breaumier, E. (2003), “Concrete Bridge Barriers Reinforced with Glass Fiber-Reinforced Polymer Composite Bars,” ACI Structural Journal, 100(6), 815-824.

Hill, C. D. and Sippel, K. D. (2002). "Modern Deformation Monitoring: A Multi Sensor Approach." FIG XXII International Congress, Washington DC, USA

Horton, R., Power, E., Van Ooyen, K., and Azizinamini, A. (2000). ‘‘High performance steel cost comparison study.’’ Proc., Steel Bridge Design and Construction for the New Millennium with Emphasis on High Performance Steel, Baltimore, 120–137.

Kuhlmann, H. and Glaser, A. (2002). "Investigation of New Measurement Techniques for Bridge Monitoring." 2nd Symposium on Geodesy for Geotechnical and Structural Engineering, Berlin, Germany

Leica Geosystems, Automated High Performance Total Station TCA2003, http://www.leica-geosystems.com

Lynch, R. J. (2004). “Provisional Design Guide in AASHTO Language for FRP Bridge Strengthening”, Master Thesis, University of Missouri - Rolla, August 2004.

McDermott, J. F. (1969): ‘‘Local plastic buckling of A514 steel members.’’ J. Struct. Div. ASCE, 5(9), 1837–1850.

Merkle, W. J. (2004). "Load distribution and response of bridges retrofitted with various FRP systems", Master Thesis, University of Missouri - Rolla, August 2004.

Nanni, A. (2003), “North American Design Guidelines for Concrete Reinforcement and Strengthening Using FRP: Principles, Applications and Unresolved Issues,” Construction and Building Materials, 17(6-7), 439-446.

Roeder, C. W., Barth, K. E., and Bergman, A. (2004). ‘‘Effect of live-load deflections on steel bridge performance.’’ J. Bridge Eng., 9(3), 259 – 267.

Roeder, C. W., Barth, K. E., Bergman, A., and Christopher, R. A. (2001). ‘‘Improved live-load deflection criteria for steel bridges.’’ NCHRP Interim Rep. No. 20-07/133, National Cooperative Highway Research Program, Washington, D.C.